NREL/TP-451-7065 • UC Category: 1263 • DE94011885

Development of High-Efficiency, Thin-Film CdTe Solar Cells

Annual Subcontract Report 1 January 1993 – 31 December 1993

A. Rohatgi, H. C. Chou, S. Kamra, A. Bhat
Georgia Institute of Technology
Atlanta, Georgia

NREL technical monitor: B. von Roedern

National Renewable Energy Laboratory
1617 Cole Boulevard
Golden, Colorado 80401-3393
A national laboratory of the U.S. Department of Energy
Managed by Midwest Research Institute
for the U.S. Department of Energy
under contract No. DE-AC36-83CH10093

Prepared under Subcontract No. XG-2-11036-3

September 1994

DISCLAIMER

TABLE OF CONTENTS

LIST OF FIGURES

LIST OF TABLES

1. Introduction

Polycrystalline thin film CdTe solar cells are one of the leading candidates for terrestrial photovoltaic applications. Theoretical calculations project an efficiency of 27% for single crystal, single junction CdTe cells, and the practically achievable efficiency for polycrystalline CdTe cells is 18-20%. Polycrystalline CdTe cells made by different groups show a significant variation in short circuit currents, open circuit voltages, and cell efficiencies. A better understanding of carrier loss and transport mechanism is crucial for explaining these differences, improving the yield, and bridging the gap between current and practically achievable limits in CdTe cell efficiencies.

The goal of this program is to improve the understanding of the loss mechanisms in thin film CdS/CdTe solar cells and to improve their efficiency by characterizing the properties of the films as well as the finished devices. In order to accomplish this goal, solar cells were fabricated on glass/SnO_2 substrates by sequentially growing CdS films from aqueous solution, CdTe films by MOCVD, and Cu/Au films by evaporation. The glass/SnO_2 substrates were supplied by Solarex Corporation and Libbey Owns Ford. Several process parameters were varied to observe their effects on cell performance. The films and the devices were characterized using Secondary Ion Mass Spectroscopy (SIMS), I-V, C-V, I-V-T and Electron Beam Induced Current (EBIC) measurements.

Rapid thermal processing (RTP), which is still a relatively new technology with growing applications in the semiconductor industry, is being investigated in this program as an alternative to the conventional $CdCl_2$ treatment and post-growth furnace anneal of the CdS/CdTe films. The RTP system allows annealing of the films for short durations at temperatures that are higher than those that can be used with the conventional furnace. This provides a tool to control inter-diffusion and defect formation at the CdS/CdTe interface.

We are also attempting to make CdTe/CdS cells comprised of single crystal CdTe films made by the "lift off" process. A comparison of these cells with the usual polycrystalline CdTe/CdS cells could help us understand some of the intricacies of the

polycrystalline material, $CdCl_2$ treatment and contact issues. The single crystal CdTe films are being grown on GaAs substrates, and then transferred to the glass/SnO_2 substrates.

Finally, consistent with the long term requirement of cost-effective large scale terrestrial applications of photovoltaics, we are investigating a solution growth technique for depositing CdTe films.

2. Fabrication of CdTe Solar Cells

CdS films were deposited on textured SnO_2/glass substrates, supplied by Solarex Corporation and Libbey Owen Ford, using solution growth starting from cadmium chloride, thiourea, ammonium chloride and ammonia. A reaction temperature of 80°C-85°C was used and CdS films about 2500 Å in thickness were produced with two consecutive runs on each substrate. The CdS/SnO_2/glass substrates were treated with $CdCl_2$ solution and annealed in a furnace at 450°C in N_2 ambient.

Prior to the CdTe deposition by MOCVD, the substrates were again annealed inside the reactor, this time in hydrogen atmosphere in a temperature range of 375°C to 475°C for eight to ten minutes. The surface modification of CdS after this heat treatment has been studied using Auger electron spectroscopy and has been reported earlier[1]. CdTe films were deposited on the annealed CdS/SnO_2/glass substrates at a temperature of 400°C. Dimethylcadmium and diisopropyltellurium were used as Cd and Te sources, respectively. The relative amounts of cadmium and tellurium in the growth ambient could be changed by controlling the temperature of the bottles that contain the metallorganic precursors and the flow rate of the hydrogen which was used as the carrier gas. A series of experiments were performed in which the Te/Cd mole ratio in the growth ambient was varied from about 0.02 to 6.

Front wall n-p solar cells, with the structure comprising glass/SnO_2/CdS/CdTe/Cu-Au, were fabricated by sequential evaporation of Cu and Au after the CdS and CdTe depositions. A number of parameters such as temperature during H_2 treatment of CdS films, Te/Cd mole ratio in growth ambient, Cu and Au evaporation rates and film thicknesses, and rapid thermal annealing conditions of CdS/CdTe films were varied to study heir effects on cell performance. Light and voltage biased quantum efficiency (QE), Auger depth profile, I-V-T, C-V, Secondary Ion Mass Spectroscopy (SIMS), and Electron Beam Induced Current (EBIC) measurements were performed to characterize the defects, material properties and carrier transport in the finished devices. The best cell efficiencies

were in the range of 11.5% to 12.0%

References

1. A. Rohatgi, International Journal of Solar Energy, Vol. 12, P 37 (1992).

3. The Impact of MOCVD Growth Ambient on Carrier Transport, Defects, and Performance of CdTe/CdS Heterojunction Solar Cells

(appeared in Journal of Electronic Materials, Vol. 23, No. 1, 1994)

H.C. Chou and A. Rohatgi
School of Electrical and Computer Engineering
Georgia Institute of Technology, Atlanta, GA 30332

Abstract

CdTe solar cells were fabricated by depositing CdTe films on CdS/SnO_2/glass substrates in various metallorganic chemical vapor deposition (MOCVD) growth ambient with varying Te/Cd mole ratio in the range of 0.02 to 15. The short-circuit current J_{sc} showed a minimum at a Te/Cd ratio of 0.1 and increased on both sides of this minimum. The open-circuit voltage V_{oc} was found to be the highest for the Te-rich growth ambient (Te/Cd ~ 6) and was appreciably lower (600 mV as opposed to 720 mV) for the stoichiometric and the Cd-rich growth conditions. This pattern resulted in highest cell efficiency (12%) on Te-rich CdTe films. Auger electron spectroscopy (AES) revealed a high degree of atomic inter-diffusion at the CdS/CdTe interface when the CdTe films were grown in the Te-rich conditions. It was found that the current transport in the cells grown in the Cd-rich ambient was controlled by the tunneling/interface recombination mechanism, but the depletion region recombination became dominant in the Te-rich cells. These observations suggest that the enhanced inter-diffusion reduces interface states due to stress reduction or to the gradual transition from CdS to CdTe. The hypothesis of reduced defect density in the CdTe cells grown in the Te-rich conditions is further supported by the high effective lifetime, measured by time-resolved photoluminescence, and the reduced sensitivity of quantum efficiency to forward/light bias.

3.1. Introduction

Polycrystalline CdTe solar cells are one of the leading candidates for cost-effective photovoltaics due to near-optimum bandgap (1.44 eV), high absorption coefficient, and manufacturability.[1] High-efficiency (>10%) polycrystalline CdTe/CdS solar cells have been made by electro-deposition,[2] physical vapor deposition,[3] close-space sublimation,[4] screen printing,[5] atomic- layer epitaxy,[6] metallorganic chemical vapor deposition (MOCVD),[7] and molecular beam epitaxy (MBE).[8] However, cells made by different groups show a significant variation in J_{sc} and V_{oc}, partly due to lack of understanding of the efficiency-limiting mechanism in the CdTe/CdS cells. For example, some cells show high V_{oc} but low J_{sc} and vice versa.[9] It is well known that imperfections such as native point defects in II-VI compound semiconductors affect the electrical properties of the materials. Cadmium telluride exhibits a significant amount of self-compensation, which limits the type and the range over which it can be doped. Therefore, in order to grow high-quality CdTe films and fabricate high-efficiency CdTe solar cells, further efforts are needed to improve the fundamental understanding of defects and loss mechanisms that control V_{oc} and J_{sc} of the CdTe cells. In this work, polycrystalline CdTe/CdS solar cells were fabricated by MOCVD by varying the Te/Cd mole ratio in the growth ambient in order to alter and investigate the impact of native defect concentration on the cell parameters. If the effect of growth ambient is translated into the films, then the Cd-rich ambient should introduce Te vacancies and the Te-rich ambient should introduce Cd vacancies in the bulk and at the interface.

3.2. Experimental techniques

Polycrystalline CdTe films with a thickness of $\sim 2.6\ \mu m$ were grown by MOCVD on n-type CdS/SnO_2/glass substrates. The Te/Cd mole ratio in the growth ambient was varied in the range of 0.02 to 15 by controlling the carrier-gas flow rates and the temperatures of the metallorganic sources in an attempt to alter the native defect concentration in CdTe films. After the CdTe deposition, CdTe/CdS structures were

treated in a $CdC\ell_2$:CH_3OH solution followed by an air anneal at 400°C for 30 min. This treatment is performed to enhance the grain growth and to improve the cell performance.[8] Ohmic back contacts were formed on the CdTe surface by sequentially evaporating 100Å Cu and 400Å Au followed by 90 min annealing at 150°C in Ar ambient. Cell fabrication was completed by etching the CdTe surface in 0.1% Br_2:CH_3OH to remove residual surface oxides, followed by a DI water rinse and N_2 blow-dry.

Several different techniques were utilized to characterize the defects, the electrical and optical properties of the CdTe films, and carrier transport in the finished devices. Cell efficiencies were measured under 100 mW/cm^2 air-mass (AM) 1.5 illumination. Auger electron spectroscopy (AES) depth-profile measurements were performed to investigate the film composition and the extent of inter-diffusion at the CdS/CdTe interface. The AES data were taken using a 3 KeV electron beam with a current of 1.0 μA. Sputter profiling was performed using a normal-incidence 4 KeV Ar ion beam at a current density of 50 μA/cm^2. The composition of the CdTe films was determined from the ratio of Cd and Te Auger signals. External quantum efficiency (QE) measurements were made using an Optronics Laboratory phase-sensitive detection system in which the samples were illuminated through the glass substrate. The bias-dependent QE measurements were performed in the wavelength range of 400-900 nm, both in the dark and under 30% AM 1.5 illumination. Dark J-V-T measurements were performed to determine the current transport mechanisms in CdTe/CdS devices. The J-V-T data were measured in the temperature range of 220-300 K at 10 K intervals. A multivariable regression analysis was used to obtain J_o, A, R_s and R_{sh} by fitting the measured J-V data to equation (1) at each temperature :

$$J = J_o[\, e^{\frac{q}{AkT}(V-JR_s)} - 1] + \frac{(V-JR_s)}{R_{sh}} \quad . \qquad (1)$$

The temperature dependence of the above parameters was used to determine the current transport mechanisms in devices fabricated with varying Te/Cd mole ratio in the growth

ambient. Time-resolved photoluminescence measurements were performed at 295 K, using 600 nm radiation from a pulse laser to determine the effective carrier lifetime in the finished devices.

3.3. Results and discussion

MOCVD growth ambient had a significant effect on the CdTe/CdS interface and the carrier transport mechanism in the CdTe/CdS solar cells. A systematic study was conducted to understand the correlation between defects, CdTe/CdS interface properties, carrier collection, and transport mechanisms by changing the Te/Cd ratios in the MOCVD growth ambient.

3.3.1 Defects, Interface, and Cell Performance

Auger depth profile and I-V measurements were performed first on the cells fabricated with different Te/Cd mole ratios in the MOCVD growth ambient. The AES measurements could not detect any change in the composition between a commercial CdTe single crystal and the MOCVD-grown polycrystalline CdTe films. The sensitivity of the AES (0.15% atomic) was also unable to resolve any differences between the CdTe films grown with different Te/Cd ratios in the MOCVD ambient (Figure 3.1). Therefore, there is no evidence of the formation of Te (or Cd) clusters and precipitates. However, the growth ambient had a significant effect on the electrical characteristics of the cells, namely J_{sc} and V_{oc}. J_{sc} showed a minimum at Te/Cd ratio of ~0.1 (J_{sc}=16 mA/cm^2) and increased on both sides (J_{sc} of 23.8 mA/cm^2 and 22.2 mA/cm^2 for Te/Cd ratios of ~6 and 0.02 respectively). In contrast to J_{sc}, V_{oc} was found to be low near the stoichiometric (Te/Cd ~ 1) and Cd-rich conditions, but increased monotonically when the Te/Cd ratio was increased to ~6 before becoming saturated (Figure 3.2). These results lend strength to the merit of Te-rich growth ambient and suggest that the difference in the parameters of the CdTe cells fabricated by various investigators, using different growth techniques and ambient, could be partly due to the difference in the

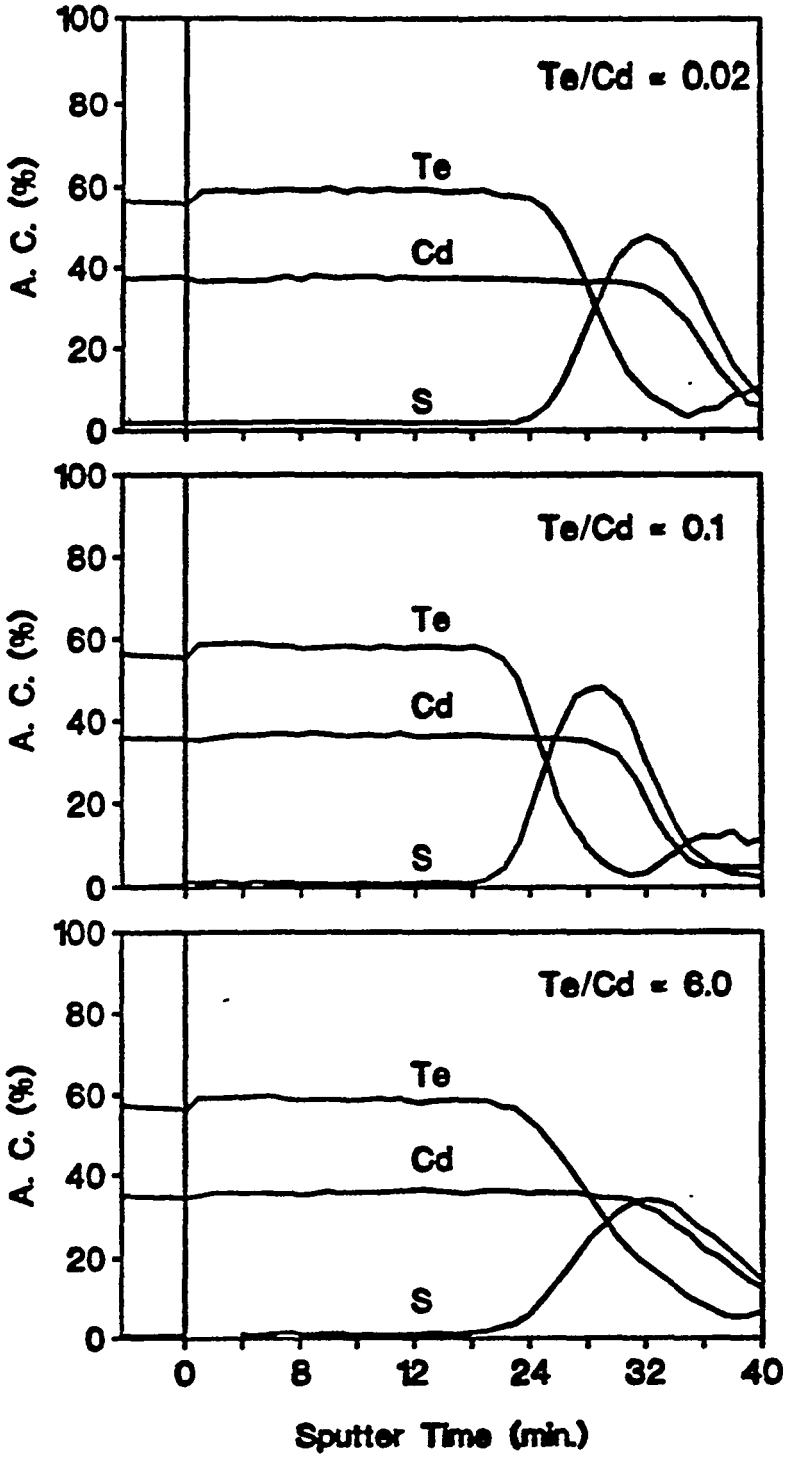

FIGURE 3.1: Auger depth profiles at and near CdTe-CdS interface for cells grown with different Te/Cd mole ratios in MOCVD ambient

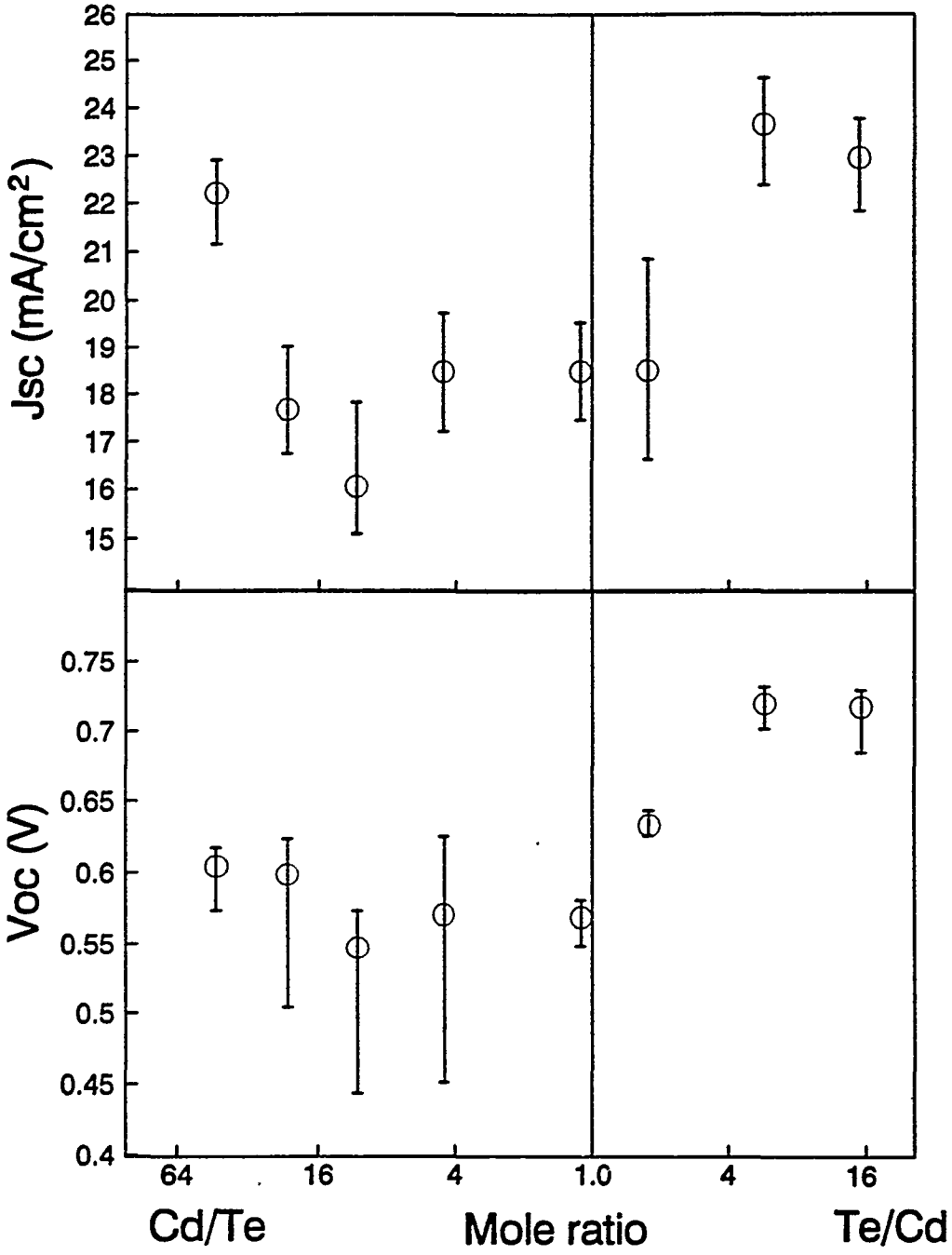

FIGURE 3.2: J_{sc} and V_{oc} of MOCVD CdTe/CdS solar cells grown with different Te/Cd mole ratios in MOCVD ambient

native defect concentration, because generally no serious attempt is made to measure or control the defect concentration.

Solar cells fabricated with three different Te/Cd mole ratios (Te/Cd ~ 6, 0.1, and 0.02) in the MOCVD growth ambient were selected for detailed analysis because (a) Te/Cd ~ 6 represents the Te-rich condition which gave the highest V_{oc} and J_{sc}, and there was no appreciable change in V_{oc} and J_{sc} when the ratio was increased to 15; (b) Te/Cd ~ 0.1 condition gave the lowest V_{oc} and J_{sc}; and (c) Te/Cd ~ 0.02 condition gave low V_{oc}, but fairly high J_{sc}.

Detailed defect and transport analysis was performed to explain the observed positive effects of Te-rich ambient on the cell performance. Even though the Auger depth-profile measurements were unable to detect the change in bulk composition, they did reveal that the atomic interdiffusion at the interface is maximum when the CdTe film is grown under the Te-rich conditions (Figure 3.1). Table 3.1 shows that the absolute efficiency of the cells grown in the Te-rich condition (Te/Cd~6) was significantly higher (11.5% as opposed to only 4.5%) than that for cells grown in the Cd-rich ambient conditions (Te/Cd~0.1). The higher V_{oc} under the Te-rich condition could be attributed to the reduction in interface states resulting from the reduced lattice mismatch due to the enhanced interdiffusion[10] or to the gradual change in bandgap from CdS to CdTe. It was also found by the AES measurements that the 400°C post-growth furnace anneal had no noticeable effect on the interdiffusion at the CdS/CdTe interface. These results indicate that the extent of interdiffusion at the interface is dictated more strongly by the MOCVD growth ambient than by the post-growth heat treatment.

The exact mechanism for enhanced inter-diffusion is not fully understood at this time. However, it is well known that the diffusion coefficient of chalcogens (Te, S etc.) in II-IV compounds increases with increasing chalcogen pressure at high temperature because under excess chalcogen conditions, fast diffusing interstitial form of the chalcogen dominates the diffusion process.[11] On the other hand, under metal (Cd) rich conditions, where the maximum chalcogen vacancy concentration are expected, the

slower vacancy-diffusion mechanism for the chalcogen dominates.[11] In addition to that, based on the observed slight decrease in the bandgap of the Te-rich CdTe films, it has been suggested that sulfur diffusion is enhanced in the Te-rich films.[12] This is based on the fact that addition of sulfur reduces the CdTe bandgap.[13] Both these facts explain the observed increase in interdiffusion at the CdS/CdTe interface grown in Te-rich conditions.

3.3.2 Light and Voltage-bias-dependent QE Analysis

Since quantum efficiency is a good indicator of J_{sc}, detailed QE measurements were performed to investigate the carrier collection probability in the cells and to explain the observed trend in the J_{sc}. QE measurements, without external light bias, on the $CdCl_2$-treated CdTe films showed no appreciable dependence on the Te/Cd ratio in the growth ambient. However, the light-biased QE showed higher carrier collection in the cells grown in the Te-rich and highly Cd-rich (Te/Cd ~ 0.02) conditions but poor carrier collection in the cells grown with Te/Cd ratio ~ 0.1 (Figure 3.3). The significant difference between dark and light QE response suggests that shining light on the CdTe solar cells activates some defects that contribute to additional recombination or carrier loss. Thus, the light-biased QE agrees well with the observed trend in the J_{sc}, and the combination of light and dark QE indicates that the Te/Cd ~ 0.1 growth condition gives rise to highest light-sensitive defect density.

It is known that the photocurrent in polycrystalline solar cells is a function of bias voltage.[14,15] Such dependence results in a decrease in collection efficiency as the bias voltage (not the light) is applied, causing a cross-over in the light and dark I-V curves. The collection probability h(V) of photon-generated carriers through the junction can be approximated by[14,15]

$$h(V) = \frac{\mu E_o}{\mu E_o + S} \quad , \tag{2}$$

where μ is the electron mobility within the junction region, E_o is the electric field across

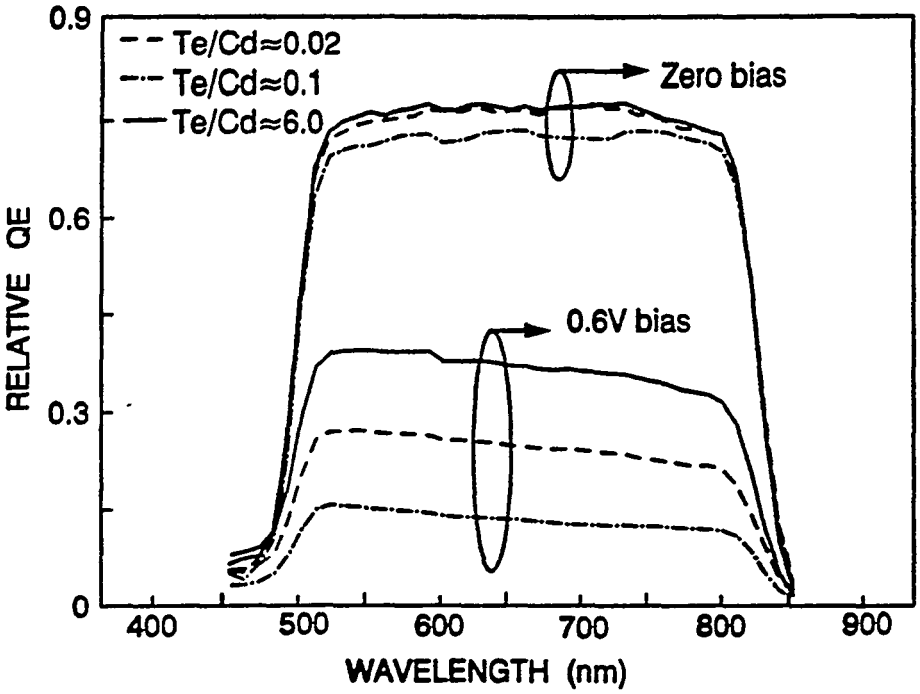

FIGURE 3.3: Light-biased quantum efficiency at zero and 0.6 V forward bias for cells grown with different Te/Cd mole ratios in MOCVD ambient

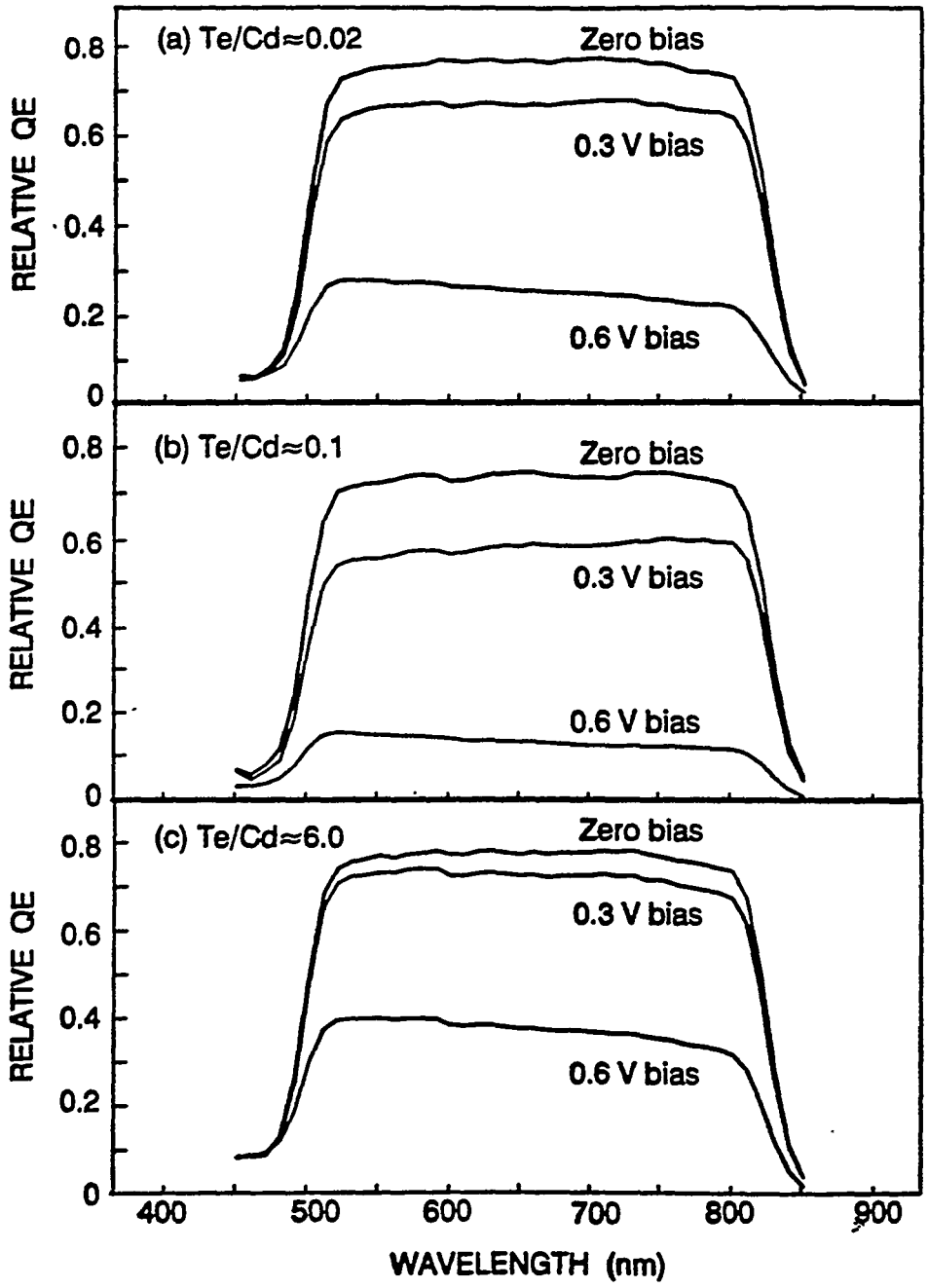

FIGURE 3.4: Change in quantum efficiency with 0, 0.3 and 0.6 volts forward bias for cells grown with different Te/Cd mole ratios in MOCVD ambient

the junction, and S is the interface recombination velocity. Since S is proportional to the interface defect density, higher defect density will result in poor carrier collection, and thus lower QE. The absolute QE as well as the relative change in QE with 0, 0.3 and 0.6 volt forward biases were measured to investigate the interface quality of the CdTe cells, as shown in Figure 3.4. Notice that the QE at any given bias is higher for the Te-rich samples. This could sometimes be due to factors other than the interface defects. However, the fact that the QE decreases rapidly with the increase in forward bias voltage and that the AES profiles show less interdiffusion for the Cd-rich CdTe cells reinforces the hypothesis of fewer defects at the CdS-CdTe interface in the Te-rich films due to the enhanced interdiffusion.

3.3.3. Carrier Transport Analysis

The general J-V characteristic of a p-n heterojunction can be described by the following equation:

$$J = J_o[\, e^{\frac{qV_j}{AkT}} - 1] \quad , \tag{3}$$

where V_j is the voltage across the junction. Carrier transport theory in heterojunctions is well documented in the literature[16-20] and will not be discussed here. However, some important points relevant to the transport analysis in this work are summarized: (a) if the diode ideality factor A, which equals $(q/kT) \times [\partial V_j/\partial(\ln J)]$, is temperature-dependent, it eliminates the possibility of transport via straight depletion region or interface recombination;[16,17] (b) if the ideality factor is temperature-independent and the activation energy (slope of $\ln(J_o T^{-2.5})$ vs 1000/T) is half of the bandgap, then the transport is dominated by depletion-region recombination and J_o can be written as[17,18]

$$J_o = \frac{q n_i W_D}{2\sqrt{\tau_{no}\tau_{po}}} = C^* T^{2.5} e^{\frac{E_g}{2kT}} \quad , \tag{4}$$

where n_i is the intrinsic carrier concentration, τ_{no} and τ_{po} are the electron and hole lifetimes in the CdTe, C^* is a temperature-independent constant, and E_g is the bandgap of CdTe; (c) if the ln J-V_j slope (=q/AkT) is temperature-dependent and J_o is thermally activated, it eliminates the possibility of direct tunneling as the dominant transport mechanism; and (d) if the current transport can be described by the tunneling/interface recombination (T/IR) model of Miller and Olsen,[19] which approximates the thermally assisted tunneling process by a series combination of direct tunneling and pure interface recombination. According to the T/IR model,

$$J = J_o[\, e^{CV_j} - 1] \quad , \tag{5}$$

where

$$J_o = J_{oo}\, e^{\frac{-\Delta E}{kT}} \tag{6}$$

and

$$C = (1-f)B + \frac{f}{(\xi kT)} \quad , \tag{7}$$

where ΔE is the thermal activation energy, B is a temperature-independent tunneling parameter, C is the slope of the lnJ vs V_j curve, and ξ represents the voltage division between the CdTe and CdS. The f parameter quantifies the extent of tunneling in the observed J-V behavior, because f=1 represents pure interface recombination with no tunneling and f=0 corresponds to direct tunneling.

Transport analysis of Cd-rich CdTe solar cells

First, the J-V-T measurements were performed on two Cd-rich CdTe cells (Te/Cd ~ 0.02 and Te/Cd ~ 0.1) that had undergone the $CdCl_2$ treatment. Ideality factor A and J_o were determined as a function of temperature, using the previously mentioned

fitting procedure. Both A and J_o were found to be temperature dependent (Table 3.2), indicating that the transport is dominated neither by pure recombination nor by direct tunneling. Therefore, an attempt was made to investigate the possibility of a tunneling/interface recombination mechanism. By fitting the experimental data to Eq. (5), the C value was determined at each temperature and then plotted as a function of 1000/T to obtain the values of (1-f)B and f/ξ. These values were found to be 20.6 V^{-1} and 0.135, respectively, for the cells grown with Te/Cd mole ratio of ~0.02 (Figure 3.5 a) and 19.2 V^{-1} and 0.254, respectively, for the Te/Cd~0.1 growth condition (Figure 3.5 b). Thus, the above analysis clearly shows that the current transport in both the cells grown in the Cd-rich ambient is limited by a combination of interface recombination and tunneling, because f is neither 0 nor 1.

TABLE 3.1: Solar cell data for CdTe/CdS cells grown with different Te/Cd mole ratios in MOCVD growth ambient

Te/Cd mole ratio	V_{oc} (mV)	J_{sc} (mA/cm^2)	FF	EFF (%)
6.0	740	23.95	0.651	11.5
0.1	593	18.80	0.425	4.5
0.02	635	22.42	0.465	6.6

TABLE 3.2: Cell parameters for cells (extracted from fit to equation 1)

T (K)	Te/Cd ~ 0.02 with $CdC\ell_2$		Te/Cd ~ 0.1 with $CdC\ell_2$		Te/Cd ~ 6 without $CdC\ell_2$		Te/Cd ~ 6 with $CdC\ell_2$	
	J_o (A/cm^2)	A	J_o (A/cm^2)	A	J_o (A/cm^2)	A	J_o (A/cm^2)	A
220	7.4×10^{-13}	2.28	8.6×10^{-14}	2.08	--		5.9×10^{-15}	1.84
230	1.7×10^{-12}	2.13	2.8×10^{-13}	2.00	--		6.2×10^{-14}	1.88
240	4.8×10^{-12}	2.02	2.4×10^{-12}	2.02	--		3.8×10^{-13}	1.87
250	3.1×10^{-11}	1.99	1.9×10^{-11}	1.98	8.7×10^{-11}	2.22	2.6×10^{-12}	1.86
260	7.4×10^{-11}	1.89	4.3×10^{-11}	1.88	3.6×10^{-10}	2.18	1.3×10^{-11}	1.89
270	2.2×10^{-10}	1.88	7.2×10^{-11}	1.74	1.6×10^{-9}	2.16	4.8×10^{-11}	1.88
280	5.5×10^{-10}	1.83	2.8×10^{-10}	1.72	6.3×10^{-9}	2.15	2.1×10^{-10}	1.89
290	1.1×10^{-9}	1.75	--		2.3×10^{-8}	2.14	7.6×10^{-10}	1.87
300	2.3×10^{-9}	1.68	--		6.8×10^{-8}	2.09	1.7×10^{-9}	1.81

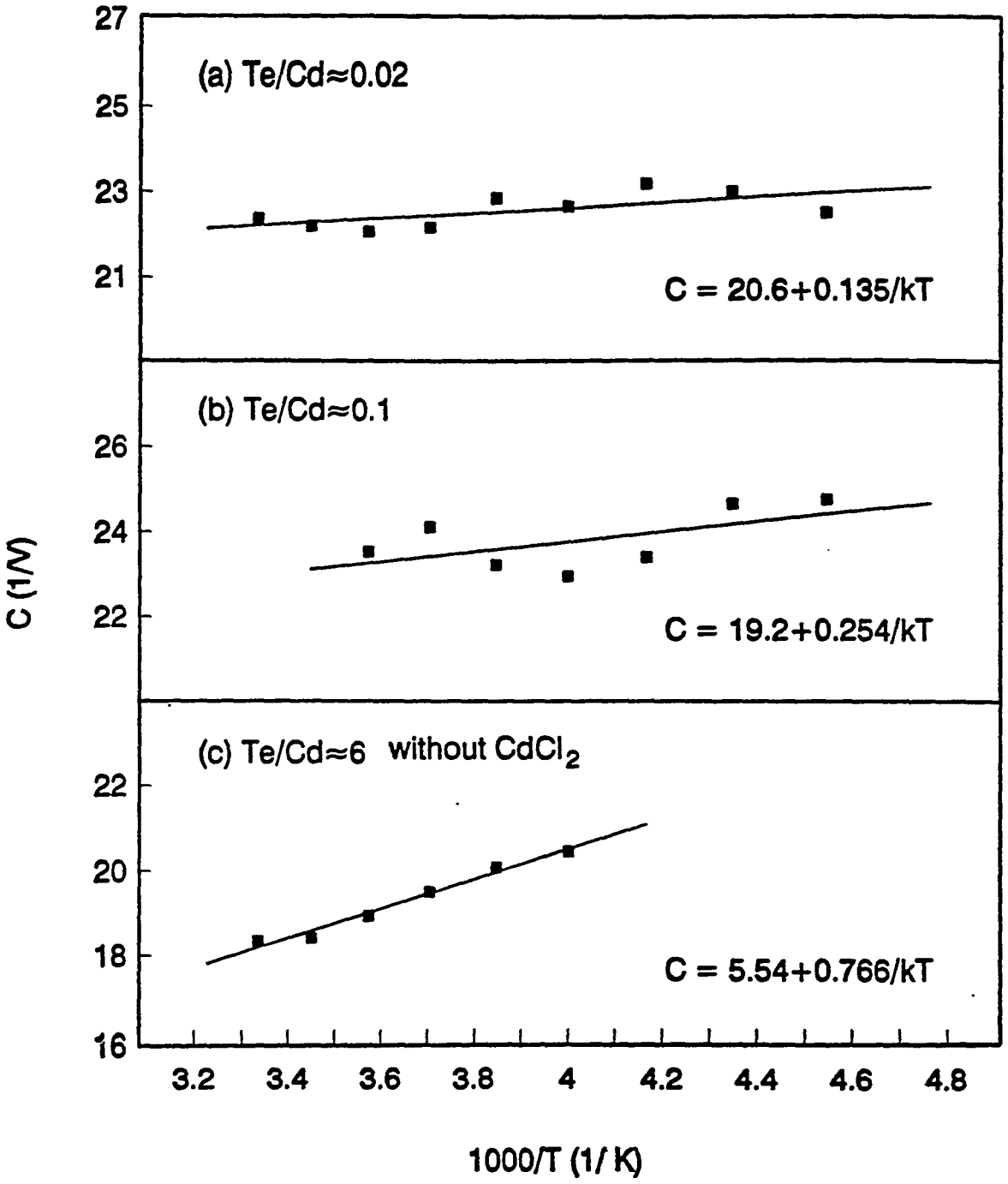

FIGURE 3.5: Plot of C-factor vs 1000/T (T/IR model), indicating that Cd-rich cells exhibit higher degree of tunneling

Transport analysis of Te-rich CdTe solar cells

The J-V-T analysis was also performed on the Te-rich (Te/Cd ~ 6) cells, with and without post-growth $CdC\ell_2$ treatment. Without the $CdC\ell_2$ treatment, both A and J_o were found to be temperature dependent; however, the A values did not change as much with temperature as was observed in the case of the Cd-rich cells analyzed above (Table 3.2). By fitting the experimental data to Eq.(6), the values of (1-f)B and f/ξ were found to be 5.54 V^{-1} and 0.766, respectively (Figure 3.5 c). Notice that the f/ξ value in the untreated Te-rich cells is higher than the value in the $CdC\ell_2$-treated Cd-rich cells. This indicates that the Cd-rich cells exhibit a higher degree of tunneling, even after the $CdC\ell_2$ treatment, compared with the untreated Te-rich cells. This again provides strong support for the hypothesis that higher atomic interdiffusion is coupled with lower defect density near the interface of the cells grown in the Te-rich condition. (Recall that most of the interdiffusion in the Te-rich samples occurs before the $CdC\ell_2$ post-growth treatment.) The tunneling probability decreases for the Te-rich cells because the enhanced interdiffusion causes the band edge to change gradually from that of CdS to that of CdTe, which not only enlarges the energy barrier thickness for tunneling but also reduces the defect density of the available tunneling sites.

After the $CdC\ell_2$ treatment, the cells grown in the Te-rich condition (Te/Cd ~ 6) showed a temperature-independent ideality factor (Table 3.2) that suggests that straight depletion-region or interface recombination controlled the current transport. Moreover, the slope of $\ln(J_oT^{-2.5})$ vs 1000/T gave an activation energy of 0.76eV (Figure 3.6), which is approximately equal to half of the CdTe bandgap, indicating that the depletion region recombination,[17,18] rather than the interface recombination, dominates the current transport in the $CdC\ell_2$-treated Te-rich cells. This result also indicates that even though the Te-rich cells have lower defect density, the $CdC\ell_2$ treatment further reduces the defect density to the extent that the transport mechanism is no longer dominated by the interface; instead, defects in the depletion region become more important. It is quite clear from this analysis that the Te-rich growth ambient combined with the post-growth $CdC\ell_2$

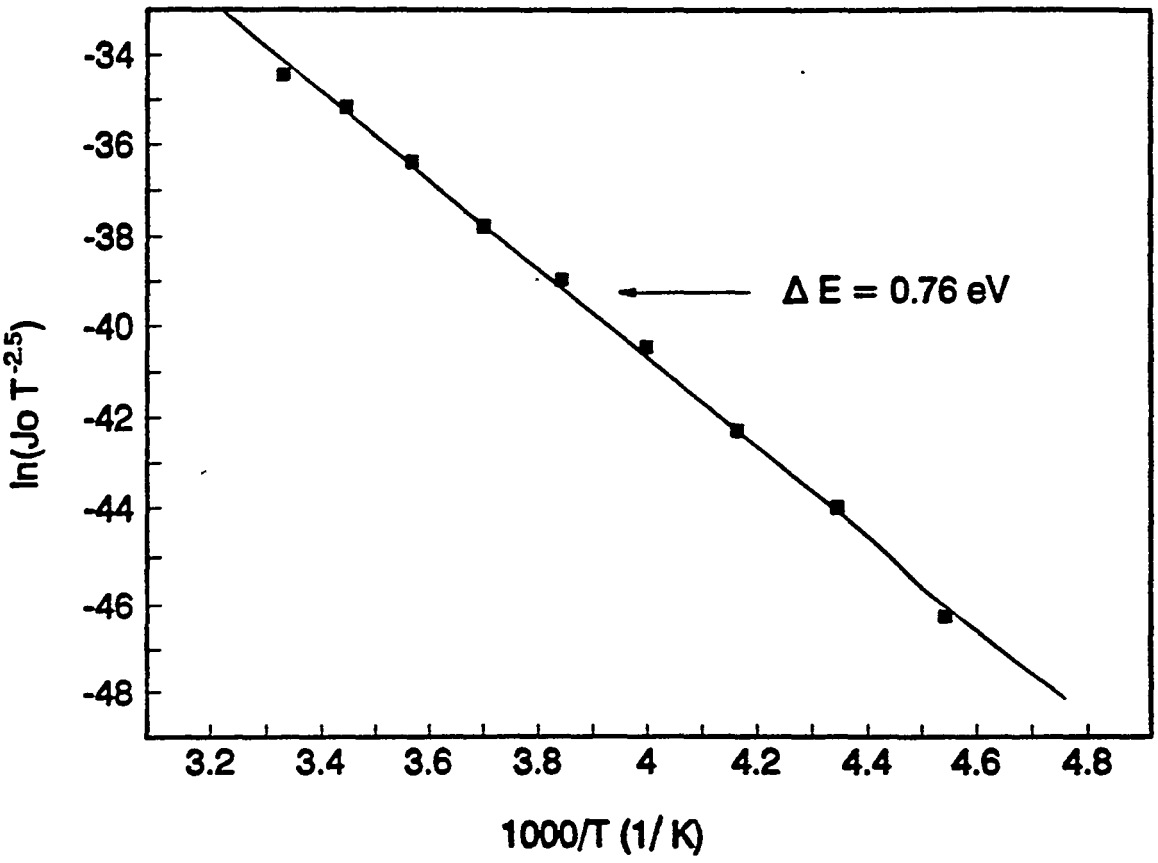

FIGURE 3.6: Plot of $\ln(J_oT^{-2.5})$ vs 1000/T for $CdCl_2$ treated CdTe/CdS cells grown in Te-rich ambient (Te/Cd~6)

treatment gives the lowest defect density, which in turn results in the best cell performance.

3.3.4 Lifetime Analysis

Photoluminescence (PL) measurements were performed in order to examine the correlation between defects, interdiffusion, and effective lifetime. The CdTe films fabricated under different Te/Cd mole ratios were studied using time-resolved PL measurements at 295 K. Table 3.3 shows the effective lifetimes, τ_e, obtained from the PL measurements on the films grown under different conditions. Note that these are effective lifetime values, which include both bulk and interface recombination. The lifetime data in the table show that both Te-rich ambient and the post-growth $CdC\ell_2$ treatment assist in improving the material quality. The Te-rich growth ambient increases τ_e from 0.116 ns to 0.153 ns, and the $CdC\ell_2$ treatment increases it further to 0.236 ns. This is entirely consistent with the cell data, because the $CdC\ell_2$-treated Te-rich devices gave the best performance. Notice that after the $CdC\ell_2$ treatment, τ_e for the Te/Cd ~ 0.02 growth condition is higher than τ_e for the Te/Cd ~ 0.1 growth condition, which agrees well with the observed trend in the J_{sc}. These results clearly indicate that the Te-rich growth condition, combined with the $CdC\ell_2$ post-growth treatment, reduces the bulk/interface defect density and accounts for the higher τ_e and improved carrier collection.

3.4. Conclusion

We have made an attempt to identify and understand some of the factors and mechanisms that affect the defects in the bulk and at the CdS-CdTe interface of CdTe solar cells. Even though we were unable to detect any differences in the film composition by AES measurements, the MOCVD growth ambient had a significant effect on the electrical characteristic of the cells. J_{sc} showed a minimum at a Te/Cd ratio of ~ 0.1 and increased on both sides of this minimum. The Te-rich growth ambient (Te/Cd $\geq$ 6) gave an average V_{oc} of 720 mV in this study, and V_{oc} was found to be about 120 mV lower for

the stoichiometric and the Cd-rich growth conditions. It is found that the Te-rich growth

TABLE 3.3: Photoluminescence lifetimes

Te/Cd mole ratio	$CdC\ell_2$ treatment	Lifetime (nsec)
0.02	No	0.116
0.1	No	0.121
6.0	No	0.153
0.02	Yes	0.210
0.1	Yes	0.201
6.0	Yes	0.236

ambient allows more interdiffusion at the CdS-CdTe interface, which in turn lowers the defect density. The post-growth $CdC\ell_2$ treatment helps in further reduction of the defect density, which results in higher τ_e, V_{oc}, J_{sc}, and cell efficiency. Reduction in the interface defect density switches the carrier transport mechanism from interface recombination/tunneling to straight depletion-region recombination in the $CdC\ell_2$-treated Te-rich devices. $CdC\ell_2$-treated Te-rich cells gave the best performance in this study, with V_{oc}=0.747 mV, J_{sc}=24.55 mA/cm^2, and efficiency =12%. These results show that process optimization coupled with basic understanding of defects and loss mechanisms is critical for improving the efficiency of CdTe solar cells.

Acknowledgement

The authors would like to thank to Dr. A. Bhat and Dr. S. Kamra for help during the cell fabrication and for useful discussions, Dr. R. R. Arya and L. Russell of Solarex Corp. for the growth of CdS and SnO_2 films, Dr. W.B. Carter of the Material Science and

Engineering Department at Georgia Tech for the help with the AES measurements, and Dr. R. K. Ahrenkiel of NREL for the PL measurements. This work was supported by NREL Contract No. XG-2-11036-3.

References

1. R. H. Bube and K. W. Mitchell, *J. Electron. Mater.* 22, 17 (1993).
2. P.V. Meyers, *Solar Cells* 24, 35 (1988).
3. R.W. Birkmire, B. E. McCandless, and J. E. Phillips, *Proc. Polycryst. Thin Film Program Review Meeting*, (SERI, Lakewood, CO, 1989), p.77.
4. T.L. Chu, S.S. Chu, and S.T. Ang, *J. Appl. Phys.* 64, 1233 (1988).
5. N. Suyama, T. Arita, Y. Nishiyama, N. Ueno, S. Kitamura, and M. Murozono, *Proc. 21st IEEE Photovolt. Spec. Conf.* (IEEE, New York, 1990), p.498.
6. J. Skarp, Y. Koskinen, S. Lindfors, A. Rautianinen, and T. Suntola, *Proc. 10th EC Photovolt. Solar Energy Conf.* (Kluwer Academic, Netherlands, 1991), p.567.
7. A. Rohatgi, H. C. Chou, A. Bhat, and R. Sudharsanan, *AIP Conf. Proc. 268: Photovoltaic Advanced Research and Development Project* (AIP, New York, 1992), p.243.
8. S. A. Ringel, A. W. Smith, M. H. MacDougal, and A. Rohatgi, *J. Appl. Phys.* 70, 881 (1991).
9. J. R. Sites, Colorado State Univ. Annual Report to NREL: *Role of Polycrystallinity in CdTe and $CdInSe_2$ Photovoltaic Cells* (1992), p.6.
10. I. Clemminck, M. Burgelman, M. Casteleyn, J. De Poorter, and A. Vervaet, *Proc. 22nd IEEE Photovolt. Spec. Conf.* (IEEE, New York, 1991), p.1114.
11. M. Aven and J. S. Prener, *Physics and Chemistry of II-VI Compounds* (Wiley, New York, 1967), p.254.
12. A. Rohatgi, S. A. Ringel, R. Sudharsanan, and H. C. Chou, *Proc. 22nd IEEE Photovolt. Spec. Conf.* (IEEE, New York, 1991), p.962.
13. R. W. Birkire, S. S. Hegedus, B. E. McCandless, J. E. Phillips, T. W. F. Russell, W.

N. Shafarman, S. Verma, and S. Yamanaka, *AIP Conf. Proc. 268: Photovoltaic Advanced Research and Development Project* (AIP, New York, 1992), p.212.

14. R. R. Potter, C. Eberspacher, and L. B. Fabick, *Proc. 18th IEEE Photovolt. Spec. Conf.* (IEEE, New York, 1985), p.1659.
15. M. Eron and A. Rothwarf, *J. Appl. Phys.* 57, 2275 (1985).
16. A. Rothwarf, *IEEE Trans. Electron. Dev.* 29, 1513 (1982).
17. J. B. Yoo, A. L. Fahrenbruch, and R. H. Bube, *J. Appl. Phys.* 68, 4694 (1990).
18. S. A. Ringel, Ph.D. Thesis, Georgia Institute of Technology (1991), p.38.
19. W. A. Miller and L. C. Olsen, *IEEE Trans. Electron. Dev.* 31, 654 (1984).
20. A. L. Fahrenbruch and R. H. Bube, *Fundamentals of Solar Cells* (Academic Press, New York, 1983), p.147.

4. Rapid Thermal Processing of CdS/CdTe Cells

Treatment of CdS/CdTe films with $CdCl_2$-methanol solution followed by a 30 to 50 minute anneal at 400°C im air has been routinely used by several groups to produce polycrystalline CdTe solar cells with efficiencies exceeding 10%[1,2,3]. Although the post-growth $CdCl_2$ treatment is known to enhance grain regrowth and significantly improve cell performance, efficiencies produced to date are below the theoretically projected value of ~18% for the polycrystalline CdTe solar cells. Amongst the possible limiting factors are: 1) defects due to the presence of an excessive amount of $CdCl_2$, and 2) undesirable diffusion related defects at the CdS/CdTe interface during the long annealing duration. In order to avoid these possible deleterious effects, we are exploring the use of Rapid Thermal Processing (RTP) for enhancing the performance of CdTe solar cells by using higher annealing temperatures and reduced annealing duration and $CdCl_2$ content.

RTP of samples having the glass/SnO_2/CdS/CdTe structure was done in a controlled O_2-N_2 atmosphere before evaporating the Cu-Au contact to complete the cells. Several parameters such as concentration of $CdCl_2$ in methanol, temperature, duration and ambient gas composition were varied.

Analysis of CdTe films using Secondary Ion Mass Spectroscopy (SIMS):

The objective of this analysis was to detect the Cl levels in the CdTe films. According to results published earlier[4], recombination in the depletion region of CdTe cells possibly occurs through Cl-related defect states that arise because of the $CdCl_2$ treatment. The depth distribution profile was obtained using Cs^+ at 12 keV to eject negative ions of Cl.

The following three samples were chosen for the study:

(a) ID#0: The CdTe/CdS films with no $CdCl_2$/heat treatment after the MOCVD CdTe growth, and after the Cu/Au evaporation.

(b) ID#7: The CdTe/CdS films treated with $CdCl_2$-methanol solution and annealed

in air at 400°C for 30 minutes. After evaporating the Cu-Au contacts, the sample was annealed at 150°C in argon for 90 minutes.

(c) ID#8: The CdTe/CdS films annealed in an O_2-N_2 mixture at 700°C for 5 seconds using a Rapid Thermal Processor. Heat treatment after evaporating the metal contacts was identical to what was used for the sample in (b) above.

SIMS data in Figure 4.1 confirm the presence of Cl in the film that was treated with $CdCl_2$. Also, as expected, the level of Cl in the RTP CdTe film is relatively low. The small traces of Cl in this film is attributed to the $CdCl_2$ treatment of the CdS film. The large Cl signal observed during the initial 20 minutes of sputtering in all samples is due to the difference in detection sensitivity in bulk CdTe and the surface layer underneath the Au/Cu contact.

In another set of experiments, RTP was done at 700°C for 5 seconds in an ambient ranging from 0% to 20% O_2 in N_2. The highest efficiency observed was 10.7% in an ambient containing 7% O_2. However, the values of the cell parameters appeared to depend on the intrinsic characteristics of the films (before RTP) and the effect of O_2 content in the ambient was not clearly evident (Table 4.1).

TABLE 4.1: Results from RTP CdS/CdTe cells

Sample ID	V_{oc} (volts)	J_{sc} (mA/cm^2)	R_s (Ω cm^2)	R_{sh} (Ω cm^2)	FF	η (%)	% O_2
E07084d1	0.77	20.8	5.4	1140	0.64	10.1	1
E07084d2	0.76	20.3	6.6	1199	0.56	8.8	1
E07085d1	0.75	21.0	4.2	884	0.64	10.2	4
E07085d2	0.76	22.2	5.0	750	0.63	10.5	4
E07083d1	0.75	22.2	3.9	858	0.64	10.7	7
E07083d2	0.74	20.5	4.9	1065	0.63	9.7	7

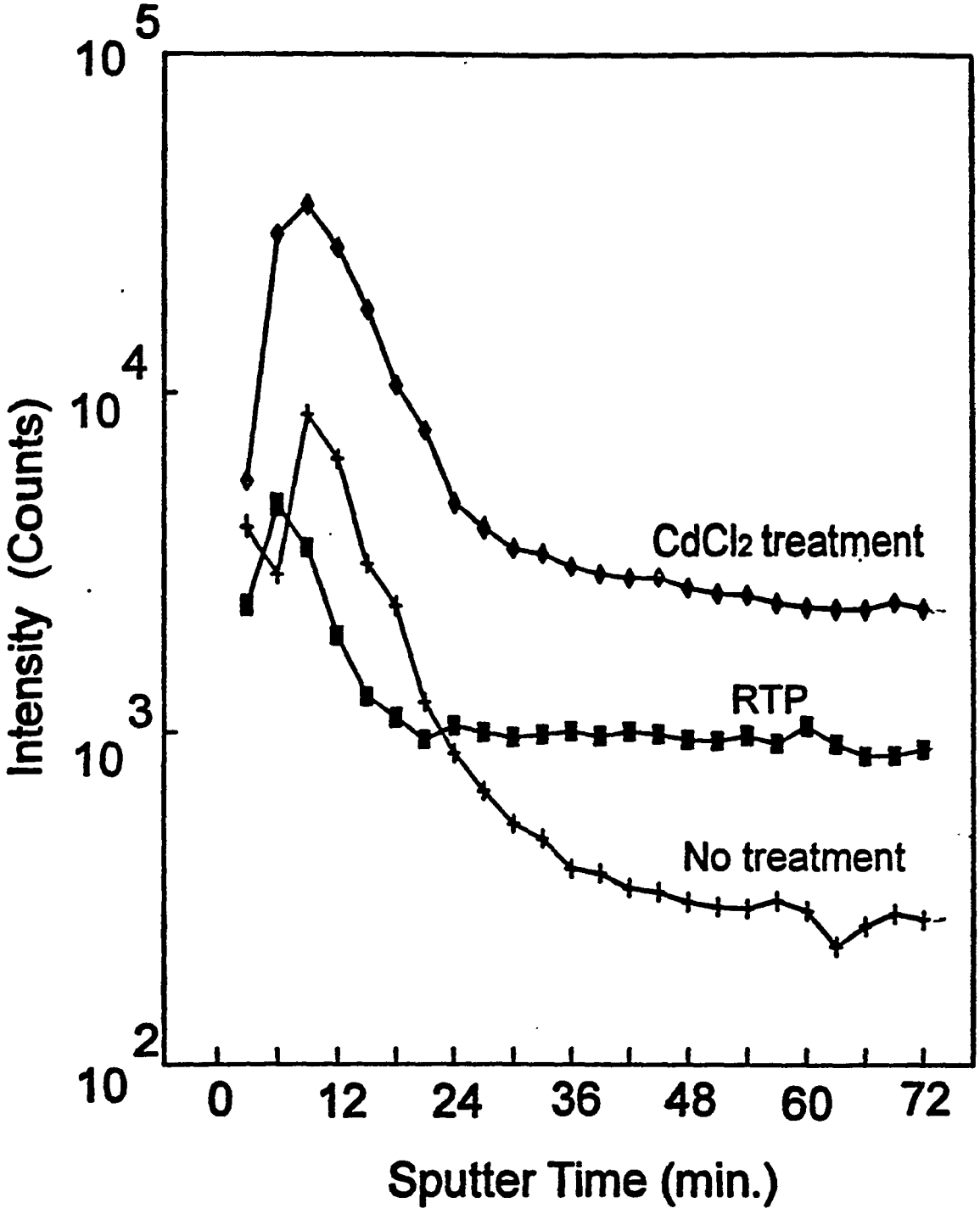

FIGURE 4.1: SIMS data showing relatively low Cl content in RTP CdTe films

It is believed that the presence of oxygen in CdTe gives rise to p-type conductivity[5]. Therefore C-V measurements were made on certain selected samples to obtain the carrier densities in the p-type CdTe films. The results are shown in Table 4.2.

TABLE 4.2: Carrier concentration in RTP cells

Sample ID	% O_2 in N_2	Carrier Concentration (cm^{-3})
E09240d1	0	3.0×10^{15}
E09241d2	10	8.1×10^{14}
E09242d1	20	1.3×10^{15}

It again appears that the effect of the O_2 content in the ambient during RTP is masked by some other variation in the characteristics of the as-grown films and the junction. Whereas the regular $CdCl_2$ and 400°C furnace anneal is known to give reasonably reproducible results, RTP cells seem to be more sensitive to and limited by the as-grown film and junction quality.

Electron Beam Induced Current (EBIC) measurements were performed by Dr. R. Matson at NREL to compare the diffusion lengths of charge carriers in CdTe films prepared using different conditions. The following three samples were used: (a) sample ID #5: as-grown film with no post-growth treatment, (b) sample ID #: film that had undergone the regular $CdCl_2$-methanol treatment and 30 min. anneal at 400°C in air, and (c) sample ID #14: film that was annealed for 5 sec at 700°C using RTP.

The SEM and EBIC scans reveal that in general the CdTe material is not very uniform in its electrical properties. Signal amplification used was different in each case and therefore the peak heights in the three cases should not be compared directly. However, it is evident (Figure 4.2) that the EBIC signal drops more gradually for the

(a)

(b)

(c)

FIGURE 4.2: EBIC signals showing diffusion lengths in CdTe films, (a) no post-growth treatment of CdTe films, (b) 30 min. anneal at 400°C in air, (c) 5 sec. anneal at 700°C in O_2-N_2 ambient using RTP, (Signal amplification is not the same for the three cases.)

annealed films (both regular furnace and RTP) than for the as-grown film as we move away from the CdS/CdTe interface into the bulk of the CdTe film. This result indicates that RTP plays a role similar to the regular furnace treatment in enhancing the life-time of the charge carriers.

We believe that the quality of as-grown films and the CdS/CdTe interface is very crucial for RTP cells, and the cell performance can be further enhanced by carefully monitoring the parameters in each of the processing steps.

References

1. B.N. Baron, R.W. Birkmire, J.E. Phillips, W.N. Shafarman, S.S. Hegedus, B.E. McCandless, University of Delaware, Polycrystalline Thin Film Materials and Devices, Annual Report to SERI, March 1991.
2. J.S. Lee, and H.B. Im, J. Mater. Sci. 21, 980 (1986).
3. J.S. Roh and H.B. Im, J. Mater. Sci. 23, 2267 (1988).
4. S.A. Ringel, A.W. Smith, M.H. MacDougal, and A.Rohatgi, J. Appl. Phys. 70 (2), 881 (1991).
5. Kiyoshi Kuribayashi, Hitoshi Matsumoto, Hiroshi Uda, Yasumasa Komatsu, Akihiko Nakano and Seiji Ikegami, Jpn. J. Appl. Phys., Vol. 22, N0. 12, pp 1828-1831, (1983).

5. Effect of Cu Film Thickness and Evaporation Rate on Cu Diffusion

5.1. Objective

Low resistance contacts between the electrodes and semiconductor films are critical for high efficiency solar cells. It is especially difficult to make a low-resistance contact to p-type CdTe for CdTe/CdS solar cells[1]. The difficulties come from the compensation mechanism of II-VI semiconductor and large work function for p-type CdTe. Several investigators have utilized Cu/Au metal films or graphite paste doped with Cu or Hg to form ohmic contact with CdTe, and have obtained reasonable cell efficiencies[1,2]. Copper seems to play an important role in the above mentioned contact because it acts as a substitutional acceptor at Cd-sites, thus increasing the doping concentration in p-type CdTe. On the other hand, Cu may also form interstitials or Cu-defect complexes which can act as recombination centers. It is also reported that Cu in CdTe can diffuse into CdS resulting in a decrease of cell performance. However, no systematic studies about the effect of Cu have been performed. Therefore, there is ample interest in investigating the effect of Cu on CdTe solar cell performance.

5.2. Results and Discussion

In order to study the effect of copper on CdTe/CdS solar cell performance, CdTe cells with 500 Å Au, 400Å Au/100Å Cu, and 200Å Au/300Å Cu contact were fabricated and the cell parameters were recorded. Cell data (Table 5.1) showed that the addition of 100 Å Cu in the CdTe cell contact reduced the series resistance significantly (2.8 as opposed to 20.46 Ω-cm^2). However, too much amount of Cu (300 Å) caused the cell to be shorted. It appears that the addition of Cu on one hand forms a better ohmic contact with CdTe, but on the other hand, the excess Cu may diffuse into the CdTe film, or even all the way to the CdTe/CdS interface. This causes shunt paths or recombination centers, which degrades cell performance.

SIMS measurements were performed to track the Cu distribution in CdTe films and

at CdTe/CdS interface. The SIMS data show that appreciable amount of Cu is present

TABLE 5.1: Cell parameters with varying Cu film thickness

Cu (Å)	V_{oc} (volts)	J_{sc} (mA/cm^2)	R_s (Ω cm^2)	R_{sh} (Ω cm^2)	FF	η
25	.73	23.20	4.72	1122	.63	10.5 %
50	.73	22.28	4.70	1104	.61	9.9 %
75	.73	23.78	3.92	886	.64	11.0 %
100	.73	24.00	3.87	426	.60	10.5 %
150	.71	22.40	3.62	272	.58	9.2 %

TABLE 5.2: Effect of Cu film thickness on J_o and A

Cu (Å)	J_o (A/cm^2)	A
50	4.4E-11	1.821
100	1.3E-11	1.612
150	1.4E-11	1.519

in the CdTe films as well as at CdTe/CdS interface after the 100 Å Cu/ 400 Å Au metallization (Figure 5.1 a). No Cu was detected in the as-grown CdTe/CdS films prior to Cu/Au metallization (Figure 5.1 c). This clearly indicates that the Cu observed in the CdTe/CdS cells is not a grown-in impurity in the CdTe films, but instead is introduced during metallization. It was also found that there are no significant changes of Cu profile in CdTe film before annealing and after 150°C/90 min annealing (Figures 5.1 a and 5.1 b). Therefore, it is reasonable to conclude that the Cu observed in the SIMS

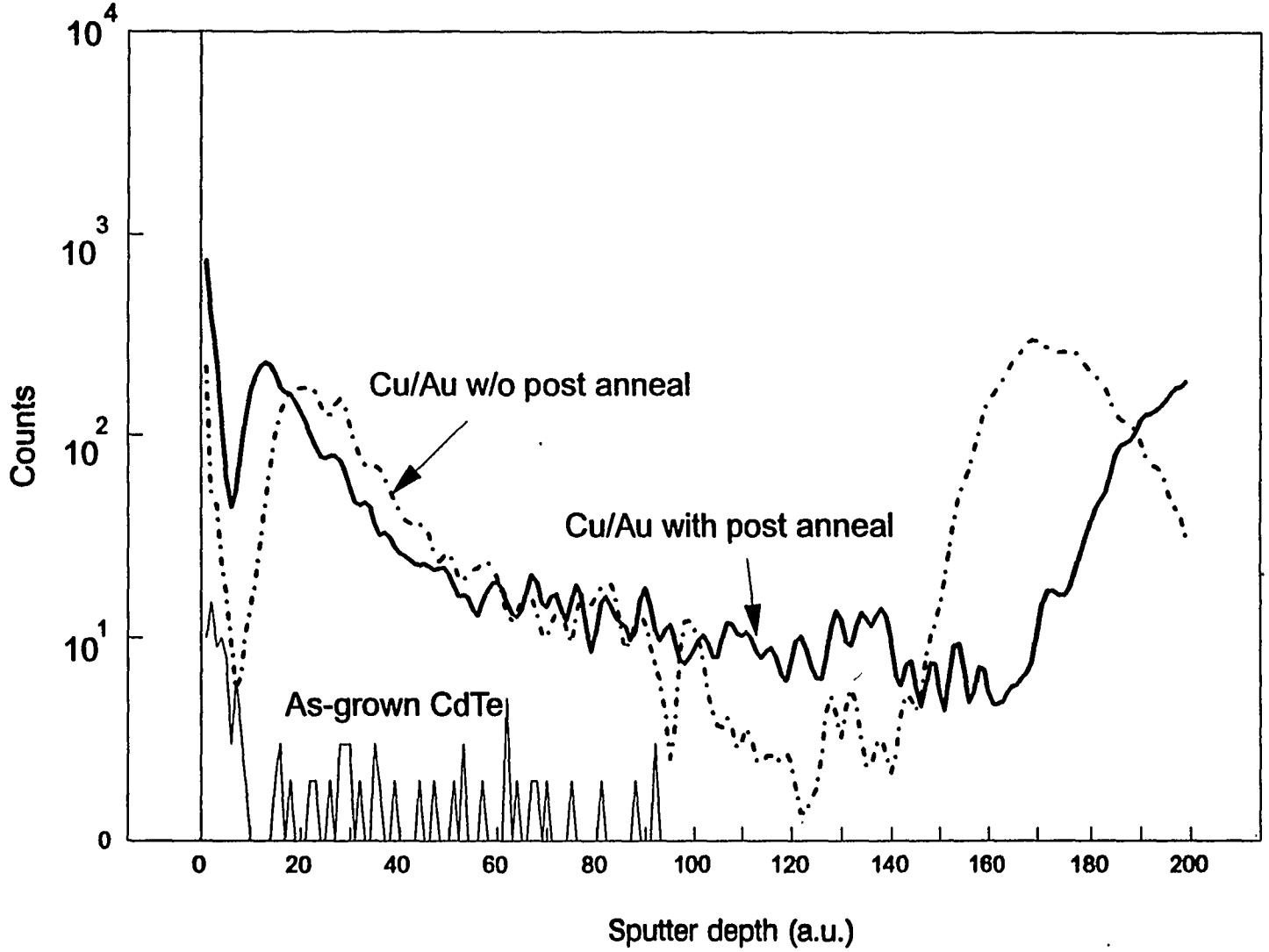

FIGURE 5.1: Cu depth profile from SIMS with and without post-growth annealing

measurements in the CdTe film and at the CdTe/CdS interface gets there via diffusion during the metallization step.

C-V measurements were performed on the CdTe cells with 500 Å Au and with 400 Å Au/100 Å Cu contact to investigate the dopant concentration in the CdTe due to Cu incorporation in the film. Figure 5.2 b shows that, like the SIMS results on Cu, the acceptor concentration decreases monotonically from the CdTe surface toward the CdTe/CdS interface for the cell with 400Å Au/100Å Cu contact. It was also found that, unlike the cells with Cu/Au contact, acceptor concentration was lower and nearly flat for the cell with only Au contact (Figure 5.2 a). Therefore, the acceptor profiles obtained from the C-V measurements must result from Cu acceptor in the CdTe films. This supports and provides the evidence of Cu diffusion into CdTe during the Cu/Au deposition to enhance the acceptor concentration and improve ohmic contact. It is worth noting that even though the measured acceptor concentration was only in the range of at 10^{15} to 10^{16}, the total Cu concentration could be much higher because of the self-compensation in the CdTe and the possibility that some Cu-related defect or complexes may not act as an acceptor even though they contribute to shunt and recombination centers.

Effect of Cu film thickness on CdTe cell performance:

The above results indicate that Cu plays a critical role in determining the CdTe solar cell performance. In order to study the optimum Cu thickness in the contact, a series of experiments were carried out by varying the Cu thickness from 0 to 150 Å in Cu/Au contact of CdTe solar cells. Cell parameters show that both R_s and R_{sh} decrease with increase in Cu thickness beyond 25 Å (Figure 5.3). It appears that the increase in Cu thickness results in better ohmic contact with CdTe, but the excess Cu causes shunt paths or recombination centers, which lower the R_{sh} and cell performance. These results further support the dual effects of Cu on CdTe cell performance. It is also found that 75 Å to 100 Å thick Cu seems to be optimal for the contact on our MOCVD grown CdTe solar cells because it gives reasonable series and shunt resistance.

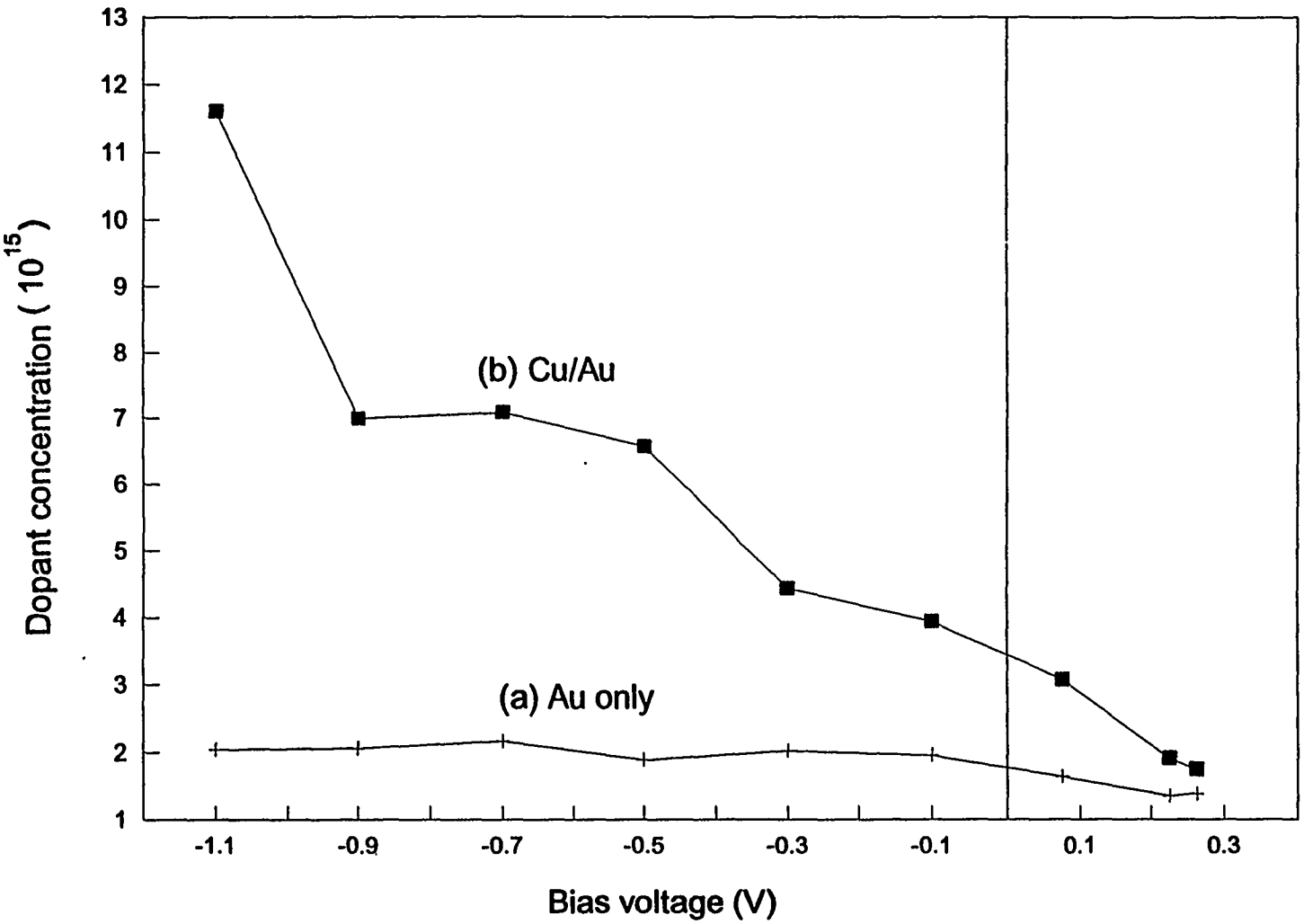

FIGURE 5.2: Carrier activation obtained from C-V data for cells with (a) Au contact and (b) Cu/Au contact

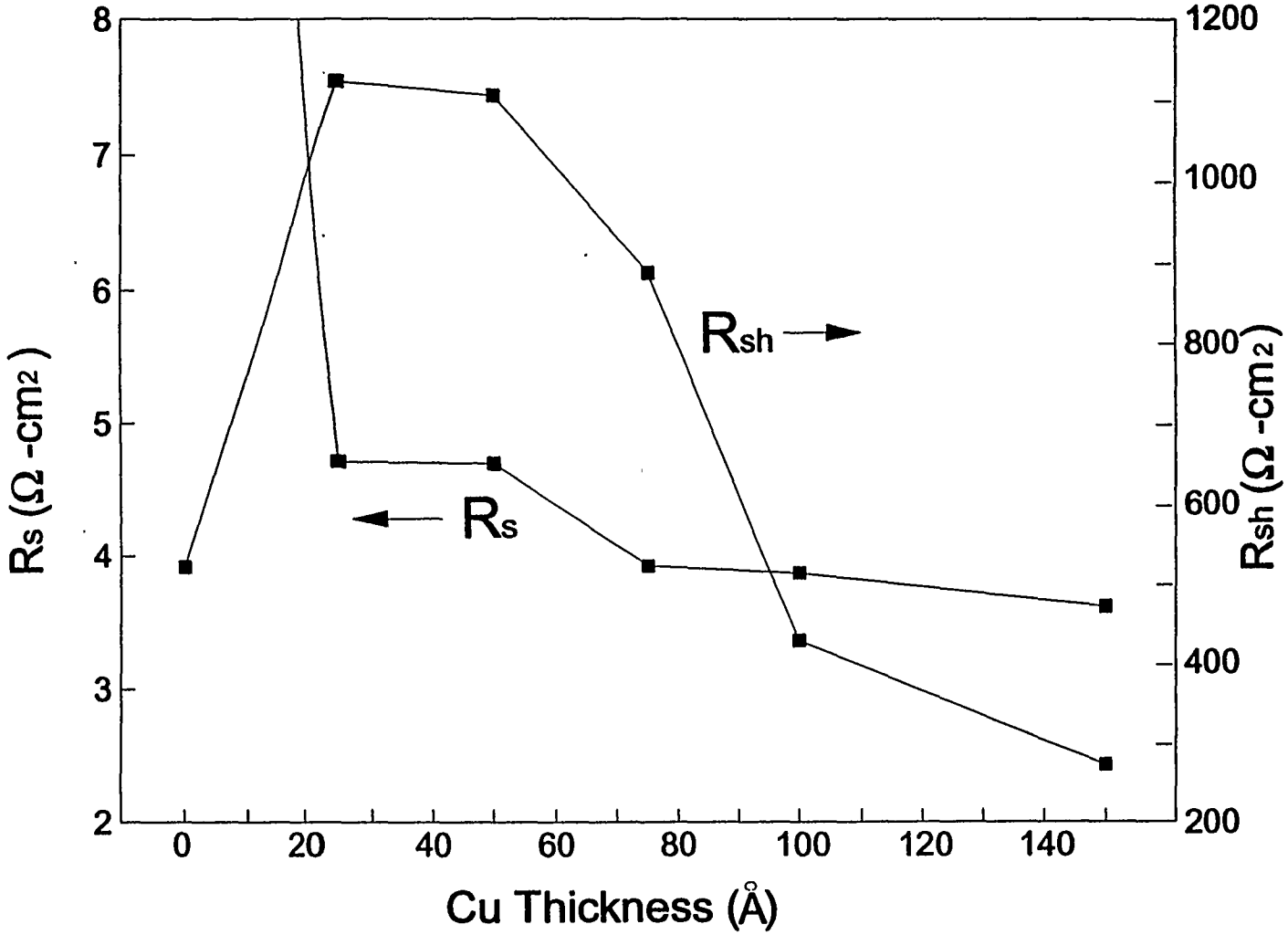

FIGURE 5.3: R_s and R_{sh} with varying Cu film thickness

SIMS measurements were performed on the cells with 50 Å and 150 Å Cu contact to investigate the correlation between the Cu film thickness and the Cu distribution in CdTe films. The results (Figure 5.4) show that the amount of Cu is higher in the CdTe films as well as at CdTe/CdS interface for the cell with 150 Å Cu contact compared to the cell with 50 Å Cu contact.

In order to understand the effects of Cu on the transport mechanism in CdTe solar cells, I-V-T measurements were performed on the cells with 50 Å, 100 Å, and 150 Å Cu contact. Ideality factors A and J_o were determined as a function of temperature, using a multi-variable regression analysis by fitting the measured J-V data to equation (1) at each temperature :

$$J = J_o[\, e^{\frac{q}{AkT}(V-JR_s)} - 1] + \frac{(V-JR_s)}{R_{sh}} \quad . \qquad (1)$$

It was found that the cells with different Cu thickness on the contact all show a temperature-independent ideality factor (Table 5.2) which suggests that straight depletion-region or interface recombination controlled the current transport. Moreover, the slope of $\ln(J_oT^{-2.5})$ vs 1000/T gave an activation energy of 0.767 eV, 0.744 eV, 0.839 eV for the cells with 50 Å, 100 Å, and 150 Å Cu contact, respectively (Figure 5.5), which is approximately equal to half of the CdTe bandgap. This indicates that the depletion region recombination, rather than the interface recombination, dominates the current transport. Therefore, even though the amount of Cu affects the shunt and series resistance, the current transport mechanism does not change.

Effect of Cu deposition rate on CdTe cell performance:

The above results indicate that the optimization of Cu/Au metallization process is critical in order to reduce the diffusion of Cu in CdTe/CdS without sacrificing good ohmic contact. Since we showed earlier that Cu thickness affects the contact resistance, Cu layer thickness was fixed at 100 Å to preserve low R_s (Figure 5.3) in the following experiments. Attempts were made to reduce Cu diffusion by changing the Cu/Au

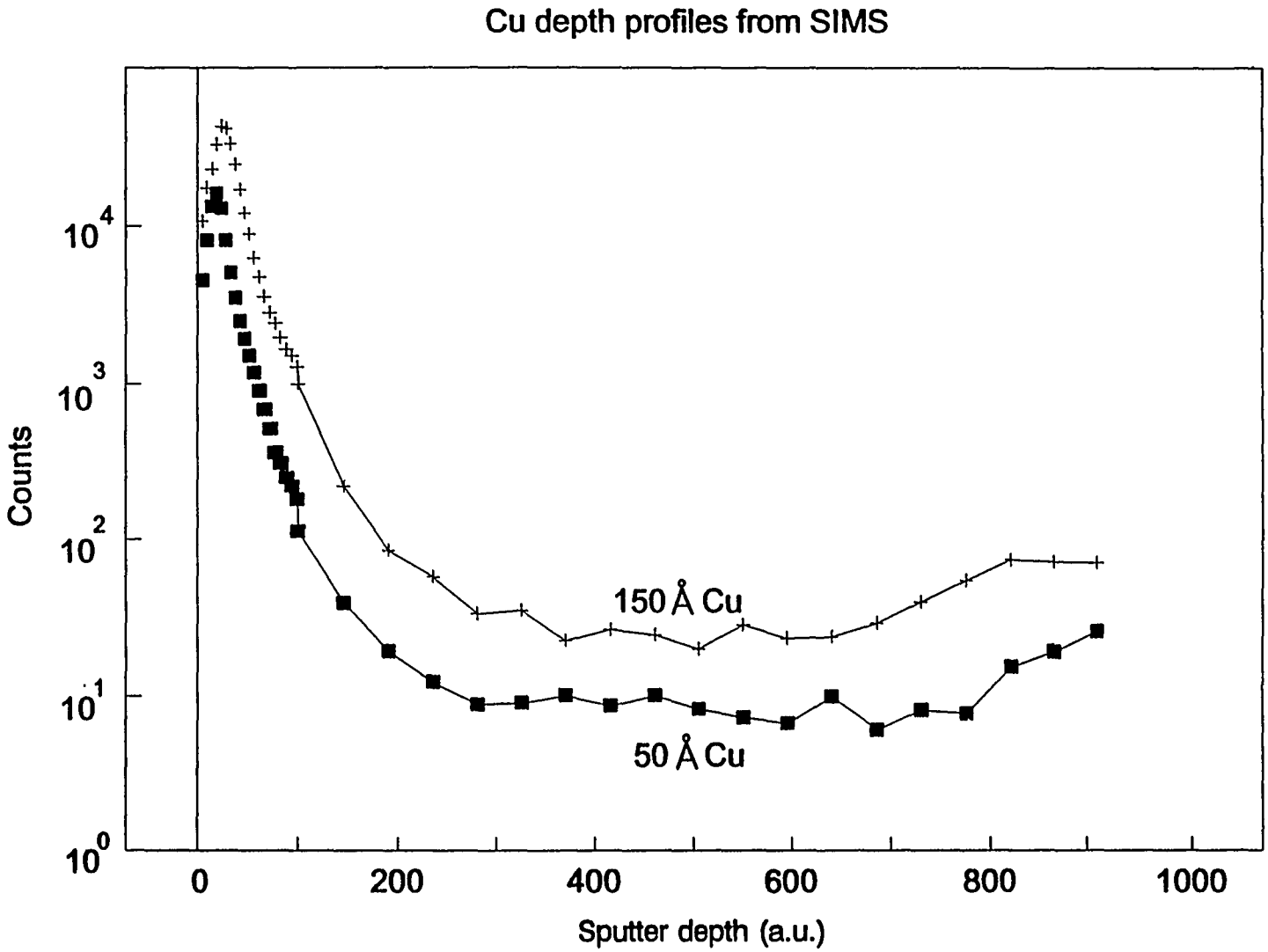

FIGURE 5.4: Cu depth profile from SIMS for Cu contacts with different thicknesses

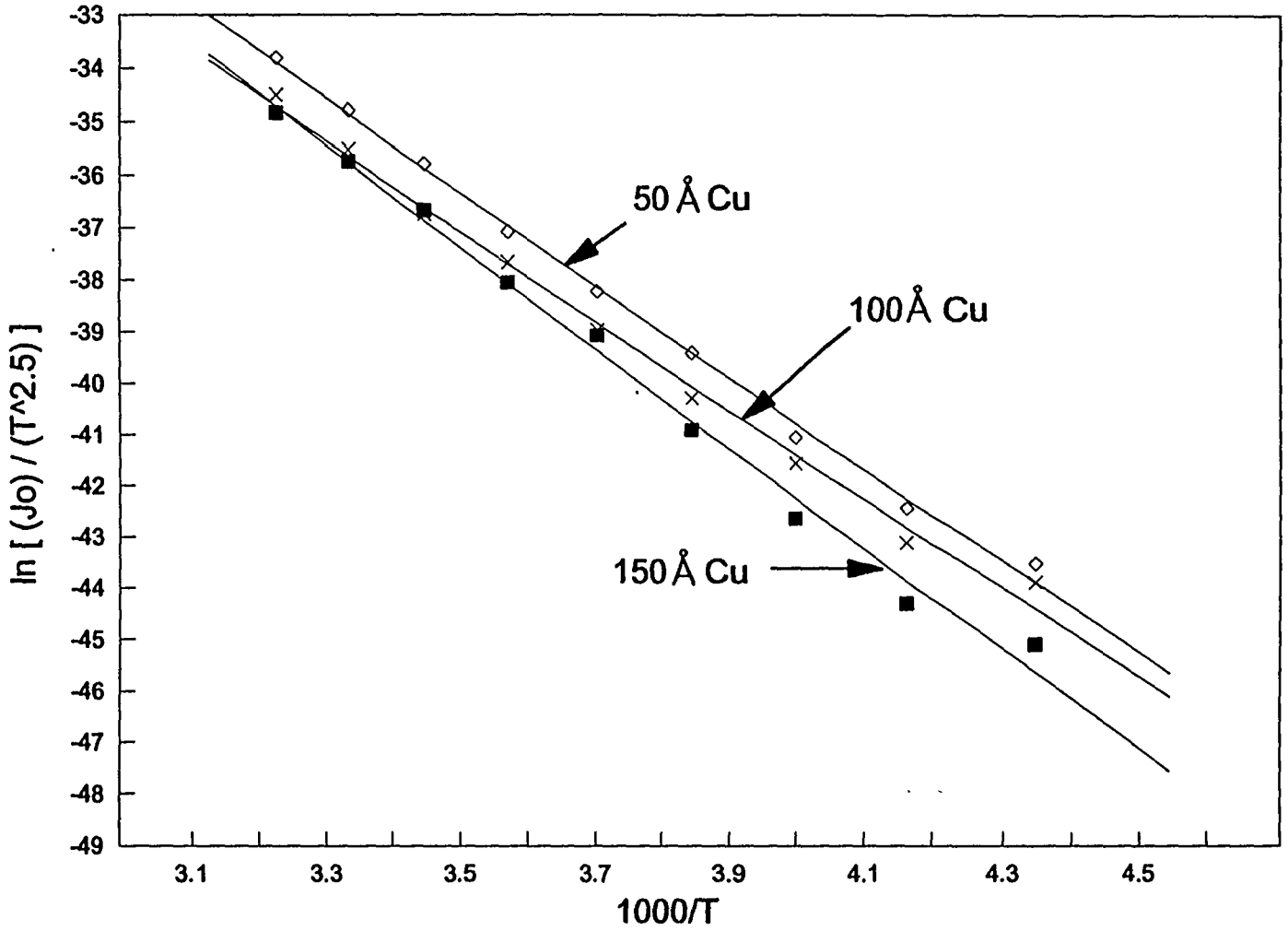

FIGURE 5.5: Plot of $\ln(J_o T^{-2.5})$ vs 1000/T for cells with different Cu film thicknesses

deposition rate during the Cu/Au metallization.

Table 5.3 shows the cell parameters of the CdTe solar cells fabricated at three different deposition rates during Cu/Au metallization. The data show that the fast Cu/Au deposition rate (1 Å/sec for Cu and 1.7 Å/sec for Au) degraded the cell performance compared to the slower Cu/Au deposition rate (0.1 Å/sec for Cu and 0.2 Å/sec for Au). The fact that R_{sh} increases as the deposition rate slows down (Table 5.3), suggests that shunt paths or recombination centers have been reduced.

TABLE 5.3: Effect of metal evaporation rate on cell parameters

	Cu/Au deposit rate 1 Å/sec, 1.7 Å/sec	Cu/Au deposit rate 0.3 Å/sec, 0.6 Å/sec	Cu/Au deposit rate 0.1 Å/sec, 0.2Å/sec
V_{oc}	0.6876	0.7262	0.7146
J_{sc}	20.776	21.673	21.356
R_s	3.94	4.49	3.44
R_{sh}	1283.83	1584.61	2007
FF	0.61	0.62	0.65
Eff	8.71	9.78	9.93
J_o	2.42×10^{-10}	1.6×10^{-10}	4.71×10^{-11}

The above hypothesis was further supported by the dark I-V measurement which revealed lower reverse saturation current density (J_o)for the cell fabricated with the slow metallization rate. In CdTe/CdS solar cells, the decrease in J_o usually represents reduction in the defect and interface state density. In order to improve the fundamental

understanding of the effect of Cu deposition rate, C-V measurements were performed on the cells to investigate the change in dopant concentration in the CdTe due to Cu incorporation in the film. Figure 5.6 shows that the acceptor concentration was larger for the cell fabricated with higher Cu/Au deposition rate. This result suggests that higher deposition rates enhance Cu diffusion.

SIMS measurements were performed in order to track the Cu distribution in CdTe films and at CdTe/CdS interface for the cells fabricated at three different deposition rates during Cu/Au metallization. No systematic change in Cu distribution in the CdTe films was found when the Cu/Au deposition rate was varied during metallization (Figure 5.7). On the other hand, relatively high amount of Cd was detected at CdTe surface in the SIMS profiles, indicating a pile-up of Cd near the surface. It was also found that for the cell fabricated with higher Cu/Au deposition rate, a larger amount of Cd piles up near the CdTe surface (Figure 5.8). The precise mechanism responsible for this phenomenon is not known, but it could be related to the microstructure of the Cu film, and the out-diffusion of Cd atoms from the CdTe film underneath. Cu is known to act as a substitutional acceptor at Cd-sites and the ability of Cu atoms to substitute Cd atoms may depend on the availibilty of Cd vacancies in the CdTe film. Therefore, the amount of electrically-active Cu atoms is higher with the higher Cu deposition rate even though the total amount of Cu does not change significantly for different Cu deposition rates. This hypothesis is supported by the C-V measurements mentioned above, which reveal a larger acceptor concentration for the cell fabricated with higher Cu/Au deposition rate. Similarly, it appears that high Cu deposition rates cause an increase in the electrically-active Cu-related defect and recombination centers that degrade the cell performance.

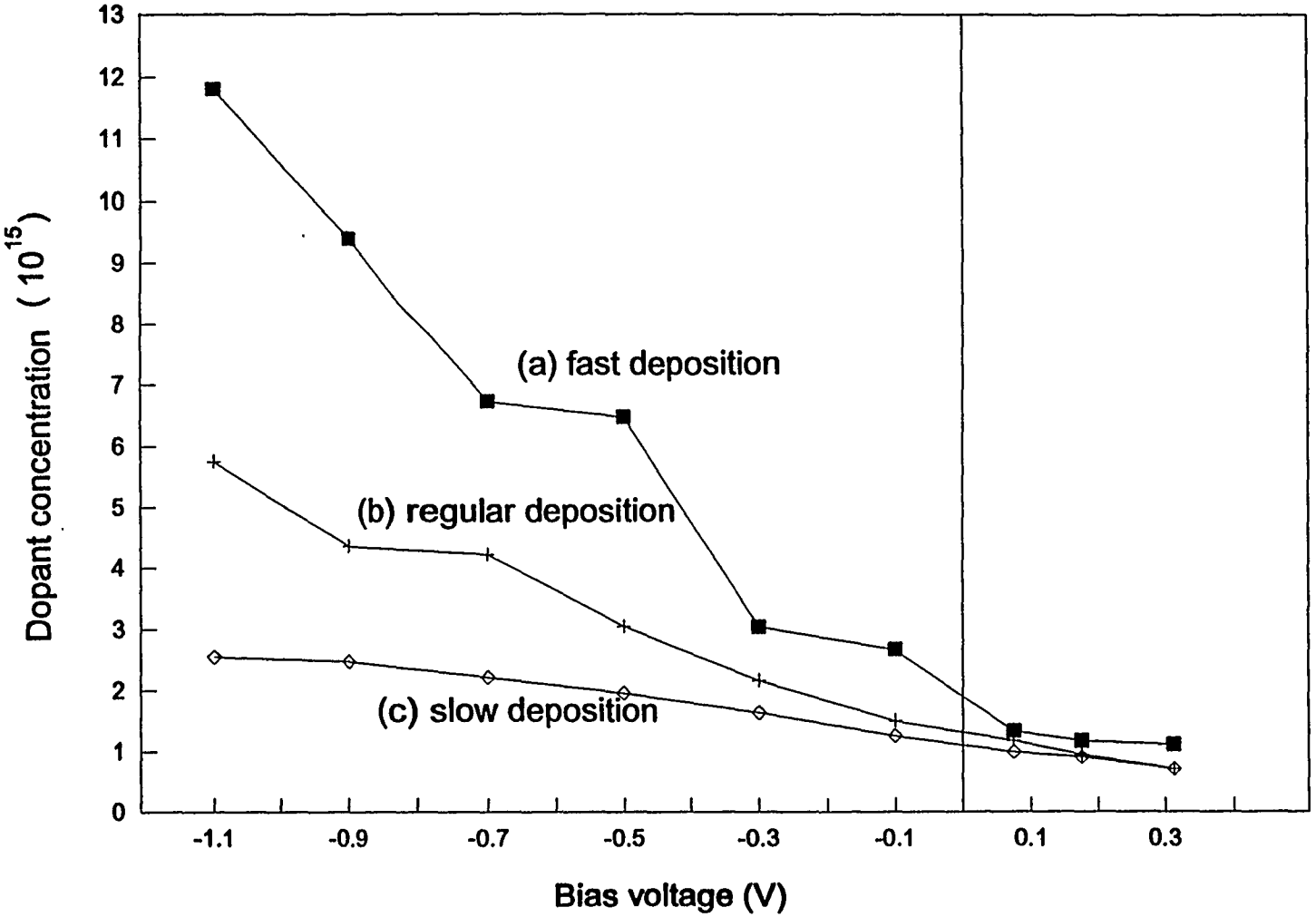

FIGURE 5.6: Carrier activation obtained from C-V data for cells fabricated using different metal evaporation rates

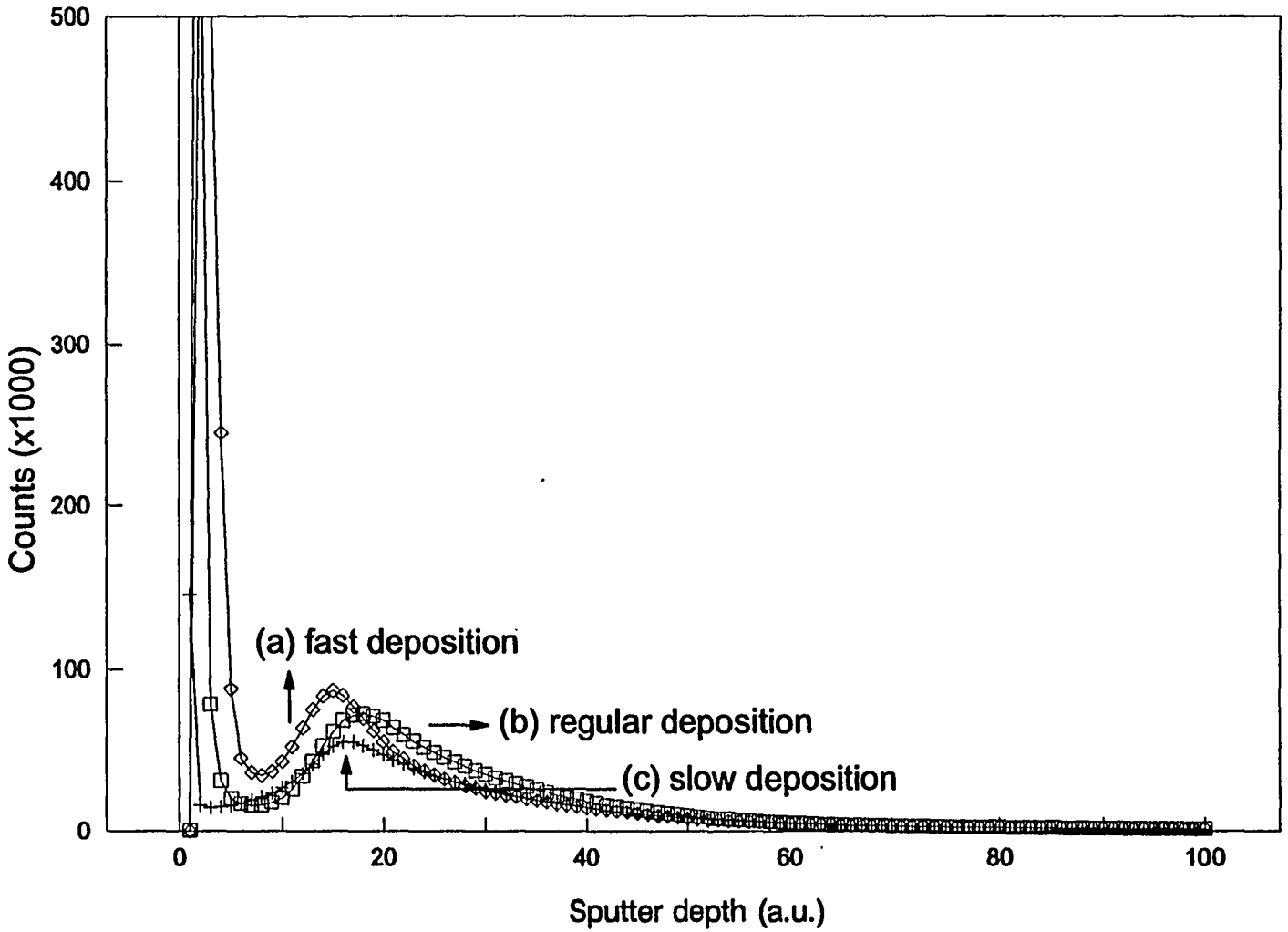

FIGURE 5.7: Cu depth profile from SIMS for cells with different metal evaporation rates

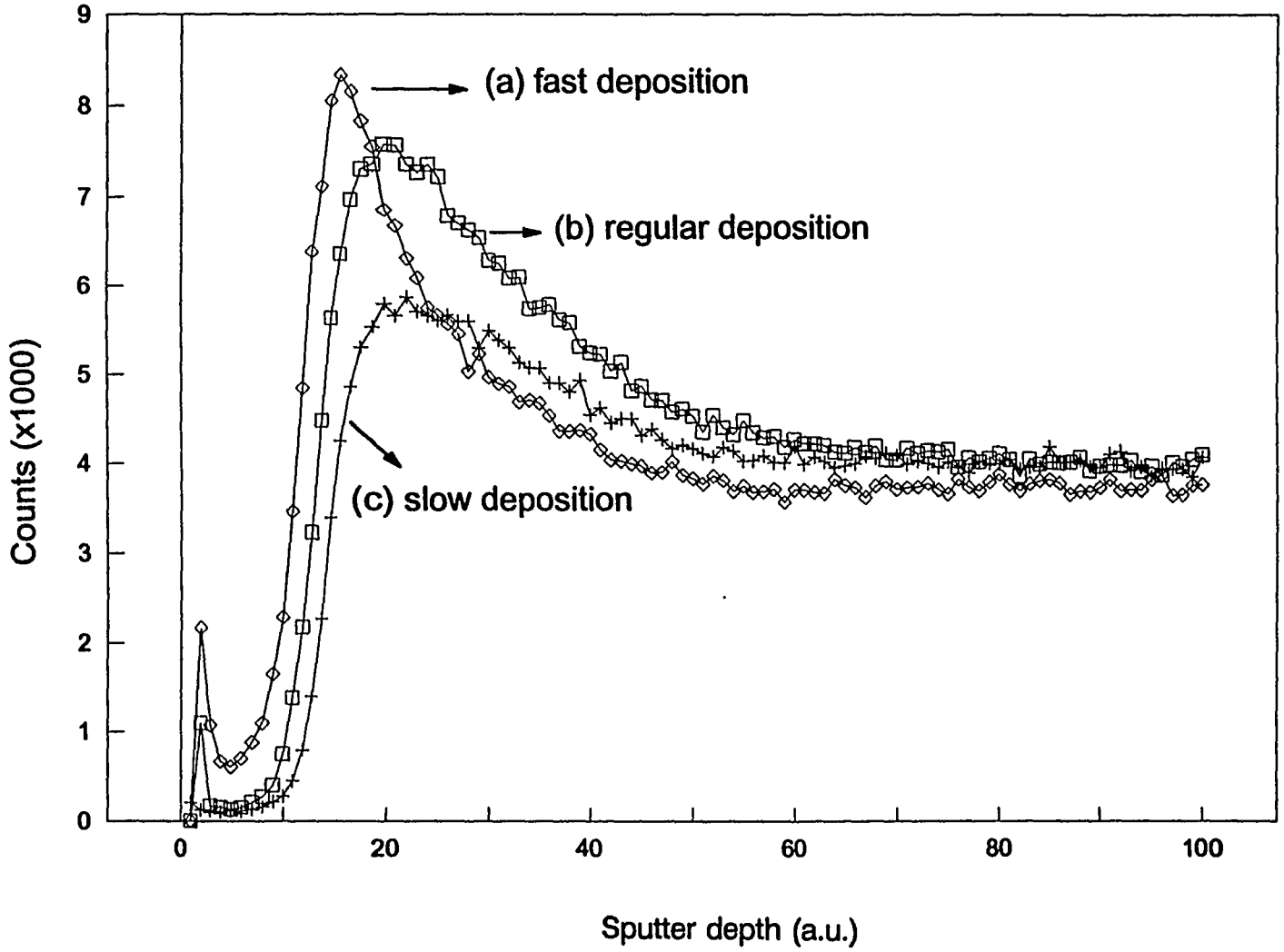

FIGURE 5.8: Cd depth profile from SIMS for cells with different metal evaporation rates

5.3. Conclusion

It was found that the addition of Cu on one hand forms a better ohmic contact with CdTe, but on the other hand, the excess Cu diffuses into the CdTe film and to the CdTe/CdS interface. This causes shunt paths or recombination centers, which degrades cell performance. This was supported by SIMS and C-V measurements that were performed to trace the Cu distribution and acceptor profile in the CdTe films. It was found that both R_s and R_{sh} decrease with increase in Cu thickness for the CdTe cells fabricated with varying Cu thickness. Depletion region recombination was found to dominate the current transport in the CdTe solar cells irrespective of the Cu film thickness in the Cu/Au contact. It was found that outward diffusion of Cd is higher for cells fabricated with higher Cu/Au deposition rate, causing a large amount of Cd pile-up near the CdTe surface. This diffusion of Cd could be related to the microstructure of the Cu/Au films which is dependent on the evaporation rates. It is possible that the high rates of Cu/Au metallization create Cd vacancies in CdTe, which then result in an increase in the electrically-active Cu-related defect and recombination centers and reduce cell performance. It might be useful to examine the microstructure of the metal films using high resolution SEM, and to determine the relationship between the microstructure and the deposition rate and substrate temperature used.

References

1. Kiyoshi Kuribayashi, Hitoshi Matsumoto, Hiroshi Uda, Yasumasa Komatsu, Akihiko Nakano and Seiji Ikegami, Jpn. J. Appl. Phys. Vol. 22, No. 12, pp. 1828-1831 (1983).
2. T.L. Chu, S.S. Chu, J. Britt, C. Ferekides, C. Wang, C.Q. Wu, and H.S. Ullal, IEEE Electron Dev. Lett., 13, pp. 3003-304, (1992).

6. An Investigation of Photocurrent loss due to Reflectance and Absorption in CdTe/CdS Heterojunction Solar Cells

(to be published)

H.C. Chou, A. Bhat, S. Kamra and A. Rohatgi
School of Electrical and Computer Engineering
Georgia Institute of Technology, Atlanta, GA 30332

Abstract

An attempt is made to understand, quantify, and reduce the reflectance and photocurrent loss in CdTe solar cells. Model calculations are performed to determine the optimum thicknesses of CdS and SnO_2 films and antireflection (AR) coating on glass that can minimize the reflectance and enhance the performance of CdTe/CdS/SnO_2/glass solar cells. Photocurrent loss due to absorption in CdS film is also calculated as a function of CdS thickness. It was found that the current loss due to reflectance and absorption is more sensitive to the CdS film when its thickness falls below 1500 Å. Model calculations show that reducing the CdS thickness from 1500Å to 600 Å increases short-circuit current density (J_{sc}) by 3 mA/cm^2 because of reduced reflectance as well as absorption. Further decrease in CdS thickness below 600 Å increases reflectance but results in higher J_{sc}, because current gain due to reduced absorption in thin CdS offsets the current loss due to higher reflectance. Model calculations also indicate that J_{sc} is not sensitive to SnO_2 thickness above 4000 Å. Finally, an optimum thickness for single layer MgF_2 AR coating on glass was calculated to be 1100 Å, which should provide an additional increase of 0.7 mA/cm^2 in J_{sc}. Some of these results are also experimentally validated in this paper.

6.1. Introduction

Polycrystalline CdTe solar cells are one of the leading candidates for cost-effective photovoltaics due to near-optimum bandgap (1.44 eV) of CdTe for single junction solar

cell efficiency, high absorption coefficient, low cost, and manufacturability.[1] Current polycrystalline CdTe/CdS thin film solar cell efficiencies are in the range of 10-15%, even though the practically achievable efficiency limit is 18-22%.[2] Unlike Si, GaAs, and InP solar cells, very limited research has been conducted to minimize the reflectance of the CdTe/CdS heterojunction devices. Typical CdTe solar cell structure consists of glass/SnO_2/CdS/CdTe/Cu/Au structure in which n-type CdS forms a p-n junction with p-type CdTe, and the SnO_2 coating is used to form ohmic contact to CdS. Since the light enters from the glass surface, CdS/SnO_2 layers between glass and CdTe could affect the reflectance of the CdTe cells. Additionally, absorption in the CdS dead layer contributes to loss of photocurrent. Recently, it was shown that the reduction of CdS thickness[3] and the use of anti-reflective coating on glass[4] can result in substantial increase in short circuit current density of the CdTe cells. However, no systematic study or analysis has been conducted to optimize the CdS, SnO_2, and AR coating thicknesses to maximize the CdTe solar cell performance. Therefore, the objective of this paper is to tailor and optimize the thickness of CdS, SnO_2, and AR coating to minimize the reflectance and photocurrent loss in the CdTe solar cells by a combination of modelling and selected experiments which involve cell fabrication and testing.

6.2. Cell Fabrication and Testing

Polycrystalline CdTe films with a thickness of ~2.6 μm were grown by MOCVD on n-type CdS/SnO_2/glass substrates. After the CdTe deposition, CdTe/CdS structures were treated in a $CdCl_2$:CH_3OH solution followed by an air anneal at 400°C for 30 min. Ohmic back contacts were formed on the CdTe surface by sequentially evaporating 100Å Cu and 400Å Au followed by 90 min annealing at 150°C in Ar ambient. Cell fabrication was completed by etching the CdTe surface in 0.1% Br_2:CH_3OH to remove residual surface oxides, followed by a DI water rinse and N_2 blow-dry. Magnesium Fluoride film was evaporated on glass for antireflection coating and the short circuit current density (J_{sc}) of the cells was measured before and after the coating under 100 mW/cm^2 air-mass

(AM) 1.5 illumination to determine its impact.

6.3. Simulation of Current Loss due to Reflectance and Absorption

Reflectance measurements were made using an Optronics Laboratory phase-sensitive detection system as a function of wavelength by illuminating the cell from the glass side. The reflectance was modeled as a function of λ by utilizing the CAMS packaged program, written by Optikos Corporation. This program can evaluate and optimize the reflectance of multilayer structures as a function of λ and incident angles. In the simulations, the glass material was assumed to be totally transparent without any interference from the interior of the glass. Therefore, the reflectance from the air/glass interface and glass/SnO_2/CdS/CdTe can be calculated independently. After obtaining the reflectance, $R(\lambda)$, from the simulation, the corresponding photocurrent loss (J_R) was calculated by summation of the $R(\lambda)$ and global spectrum flux $F(\lambda)$ product in the wavelength range of 4000 Å to 9000 Å, assuming 100% internal quantum efficiency and recognizing that the bandedge of CdTe corresponds to λ=9000Å:

$$J_{R\ loss} = \sum_{\lambda=4000}^{\lambda=9000} R(\lambda) \times q \times F(\lambda). \qquad (1)$$

The photocurrent loss due to the absorption (J_A) in the CdS layer was calculated by

$$J_{A\ loss} = \sum_{\lambda=4000}^{\lambda=5100} (1 - e^{-\alpha(\lambda) \times d}) \times q \times F(\lambda)\ , \qquad (2)$$

where d is the thickness of CdS layer, $\alpha(\lambda)$ is the absorption coefficient of the CdS film.[5]

6.4. Theory and Modeling of Reflectance

For a single film with refractive index of n_1 and thickness d_1 on a substrate, the

minimum reflectance occurs at wavelength λ when $n_1 d_1 = \lambda/4$ and the corresponding minimum reflectance value is given by[6]

$$R_{min} = \left(\frac{n_1^2 - n_0 n_2}{n_1^2 + n_0 n_2} \right)^2 , \tag{3}$$

where n_s and n_0 represent the refractive index of the substrate and surrounding ambient. Two layer AR coating can reduce the reflectance further. This can be accomplished either by a narrow-band, single-minimum (V-coating) or by a broad-band, double-minima (W-coating) in the reflectance curve.

The reflectance of a two layer coating is given by[7]

$$R = \frac{X}{1+X} , \tag{4}$$

where

$$X = \frac{n_s}{4n_M} \left\{ \left[\left(\frac{n_M}{n_s} - 1 \right) \cos\phi_1 \cos\phi_2 + \left(\frac{n_1}{n_2} - \frac{n_M n_2}{n_s n_1} \right) \sin\phi_1 \sin\phi_2 \right]^2 \right. \tag{5}$$
$$\left. + \left[\left(\frac{n_M}{n_1} - \frac{n_1}{n_s} \right) \sin\phi_1 \cos\phi_2 + \left(\frac{n_M}{n_2} - \frac{n_2}{n_s} \right) \cos\phi_1 \sin\phi_2 \right]^2 \right\} ,$$

and n_1 is the refractive index of the film next to the surrounding medium (n_M), n_2 is the refractive index of the film next to the substrate (n_s), $\phi_1 = 2\pi n_1 d_1/\lambda$, and $\phi_2 = 2\pi n_2 d_2/\lambda$.

For the V-coating, the values of R and X are set to zero to realize single minimum, which leads to

$$\tan^2\phi_1 = n_1^2 \frac{(n_M - n_s)(n_s n_M - n_2^2)}{(n_s n_1^2 - n_M n_2^2)(n_s n_M - n_1^2)}, \qquad (6)$$

and

$$\tan^2\phi_2 = n_2^2 \frac{(n_M - n_s)(n_s n_M - n_1^2)}{(n_s n_1^2 - n_M n_2^2)(n_s n_M - n_2^2)}. \qquad (7)$$

The film thicknesses d_1 and d_2 for zero reflectance at a desired wavelength could be obtained from the above two equations. However, for the double minima W-type coating, a half wave thick film ($n_2\ d_2 = \frac{1}{2}\lambda$) is inserted between a quarter wave thick top layer ($n_1\ d_1 = \frac{1}{4}\lambda$) and the substrate in order to get broad reflectance spectrum with two minima.[8]

6.5. Results and Discussion

6.5.1 Theoretical Optimization of CdS and SnO_2 Thicknesses for Minimum Reflectance:

Since CdS and SnO_2 films act as double-layer coating between the glass and CdTe material in the glass/SnO_2/CdS/CdTe cell structure, detailed model calculation were performed to investigate how their thickness affect the reflectance of the device. In order to achieve the single minimum V-type reflectivity, the optimum thicknesses of CdS and SnO_2 were determined from equations (6) and (7) by substituting the appropriate refractive index values, n_M = 1.5 (glass), n_1 = 1.8 (SnO_2), n_2 = 2.5 (CdS), and n_s = 2.9 (CdTe),[9,10] which gave

$$\phi_1 = \frac{2\pi n_1 d_1}{\lambda} = 1.519 + \frac{k\pi}{2}, \quad \phi_2 = \frac{2\pi n_2 d_2}{\lambda} = 0.24 + \frac{k\pi}{2}, \qquad (8)$$

where k is an integer. If 6000 Å is selected to be the target wavelength (near the solar

spectrum peak) for the single minimum, the SnO_2 thickness d_1 should be 805.8 Å with corresponding CdS thickness d_2 of 575.6 Å. As mentioned previously, double minima (W-type) reflectance could be achieved by choosing half wavelength thick CdS (n_2d_2 = 1/2 λ, d_2=1200 Å) in conjunction with quarter wavelength thick SnO_2 (n_1d_1 = 1/4 λ, d_2=1666 Å). However, these theoretically calculated optimum thicknesses of CdS and SnO_2 for minimum reflectance may not be fully compatible with the requirements of high-efficiency solar cells. For example, SnO_2 should be sufficiently thick ($\gg$ 800 Å) to prevent power loss associated with series resistance, which can degrade fill factor and cell performance; and the CdS thickness must be sufficient ($\geq$ 600 Å) to ensure uniformity and prevent the formation of pin-holes, which can result in low shunt resistance or fill factor. On the other hand, if the CdS film is too thick, then the absorption could lower J_{sc} and cell efficiency. Therefore, further reflectance simulations and measurements were performed on glass/SnO_2/CdS/CdTe cells to determine what combination(s) of the SnO_2 and CdS thicknesses can minimize reflectance and absorption losses while maintaining the requirements for high-efficiency cells, namely low series resistance and reduced pin-hole density.

6.5.2 Practical optimization of CdS thickness including reflectance, absorption, and other requirements for high efficiency cells

Thick SnO_2 layers are necessary to reduce series resistance of CdTe cells, therefore, simulations were performed by fixing the SnO_2 thickness at 10000 Å and varying the CdS thickness in the range of 100 Å to 3000Å. The corresponding photocurrent loss due to the reflectance (J_R) was calculated for each CdS thickness (Figure 6.1 a) by using equation (1) and the simulated reflectance R(λ). It is important to recognize that a number of investigators use about 10000 Å SnO_2 to lower R_s and CdS thickness in excess of 1000 Å to avoid pin-hole problems. Figure 6.1 a shows that reducing the CdS thickness from 1500 Å to 600 Å reduces photocurrent loss by 0.77 mA/cm^2 (2.74 mA/cm^2 as opposed to 1.97 mA/cm^2) due to reduced reflectance alone,

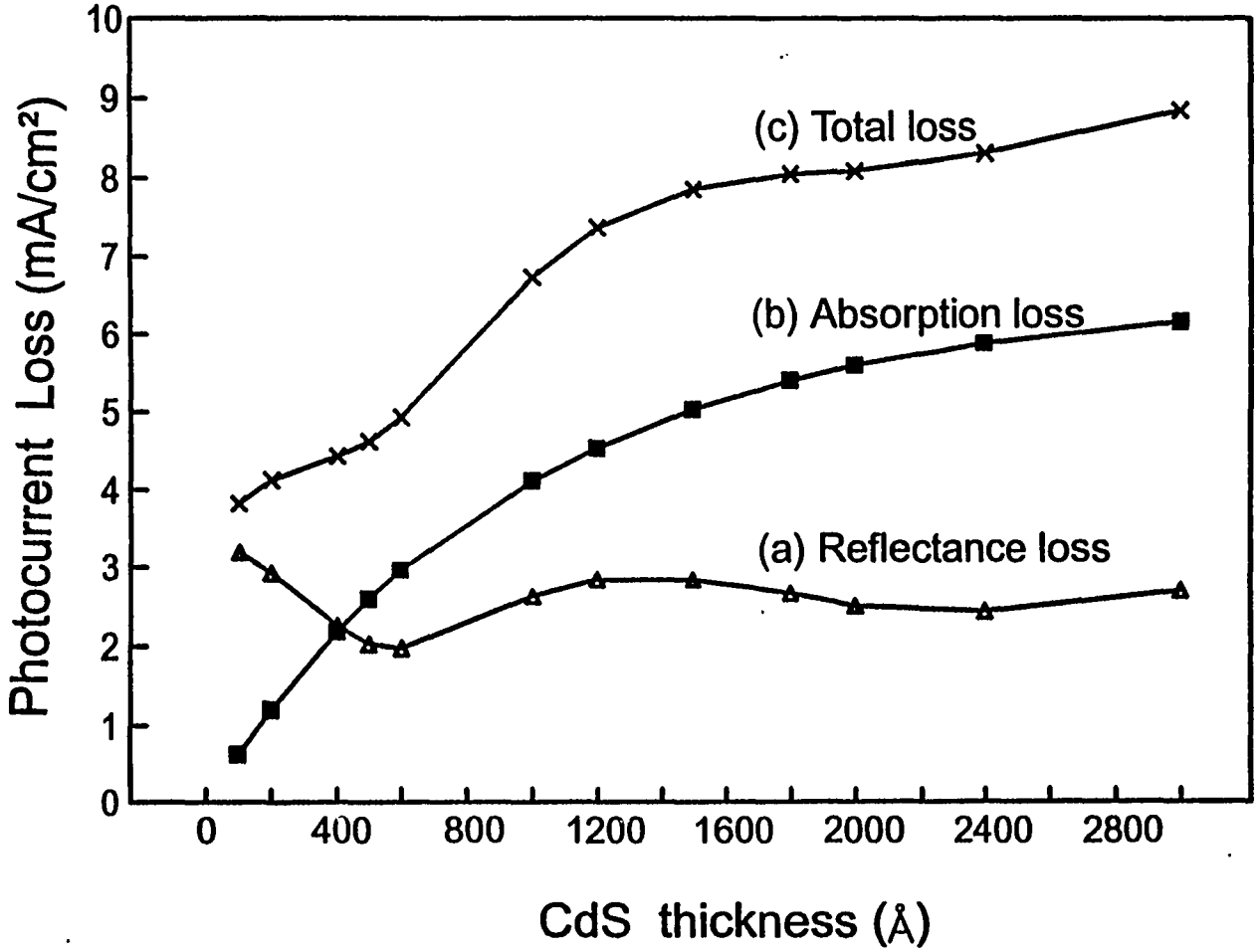

FIGURE 6.1: Simulated photocurrent loss in CdTe solar cells due to absorptionin in CdS window layer and reflection

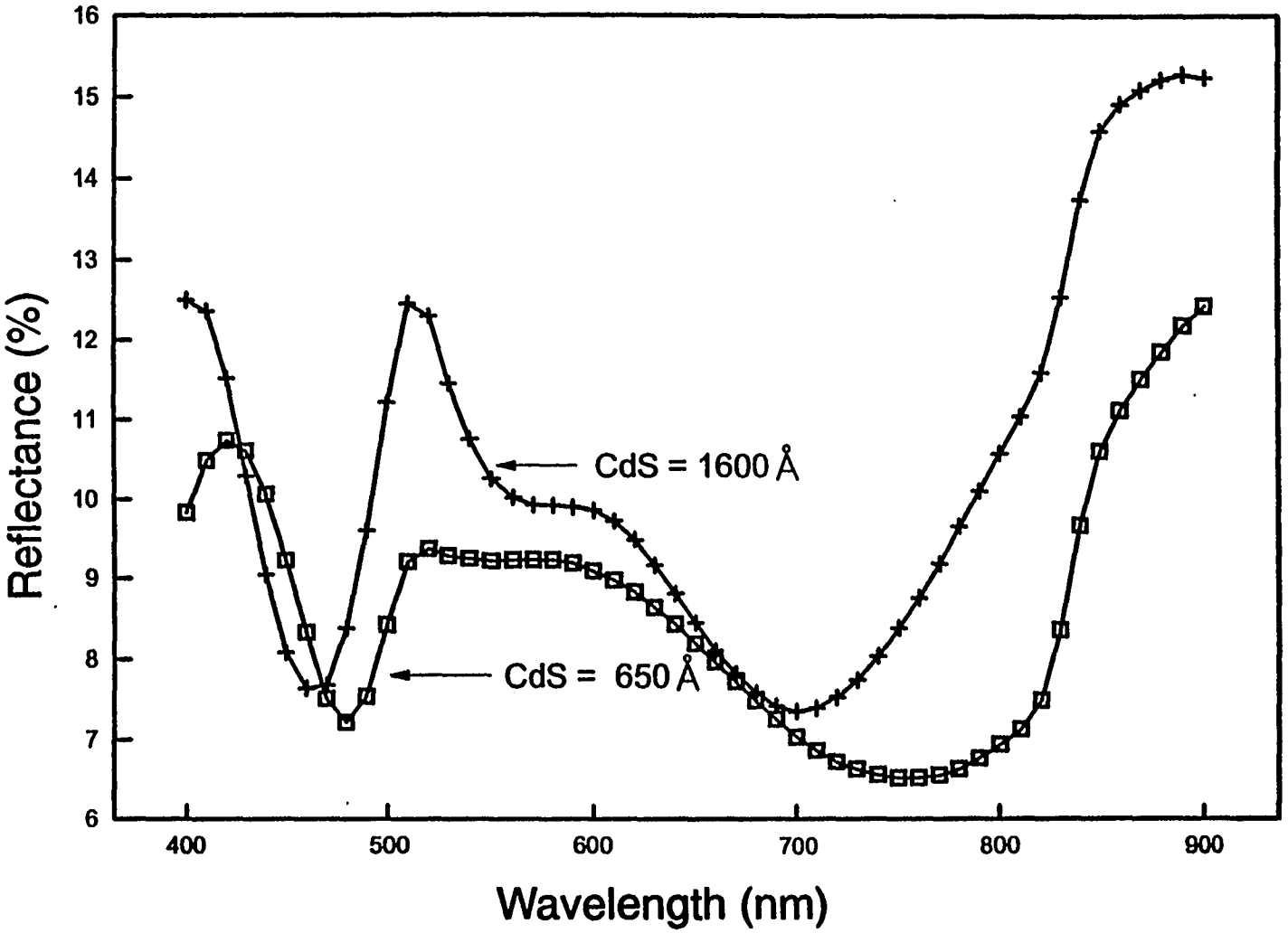

FIGURE 6.2: Measured reflectance for CdTe/CdS solar cells with different CdS thicknesses

without accounting for the absorption. In order to support the above prediction, CdTe solar cells were fabricated with 650 Å and 1600 Å thick CdS layers and their reflectance was measured. Experimental data in Figure 6.2 clearly indicates that the reflectance of the cell with 1600 Å CdS is much higher than the one with 650 Å CdS. Measured reflectance was utilized to calculate the photocurrent loss by using equation (1). Reflectance-induced current loss in the cell with 1600 Å thick CdS was found to be 0.5 mA/cm^2 higher than the cell with 650 Å thick CdS.

Figure 6.1 a shows that the current loss due to reflectance is more sensitive to the CdS film when the thickness falls below 1500 Å. This is important because generally the CdS thickness is decreased in order to reduce the photon absorption loss but the contribution due to the change in reflectance can not be ignored. For example, Figure 6.1 shows that decreasing the CdS thickness to 600 Å reduces reflectance as well as absorption losses. However, the reduction in CdS thickness below 600 Å decreases the photon absorption in the CdS layer which should improve J_{sc}, but it also increases the reflectance which should reduce J_{sc}. In order to understand and quantify the competition between absorption and reflectance losses, the photocurrent loss due to the reflectance (Figure 6.1 a) and absorption (Figure 6.1 b) were calculated with varying the CdS layer thickness in the range of 100 Å to 3000Å. It is clear that the current loss due to absorption is dominant and decreases rapidly with the decrease in CdS thickness. It is interesting to note that the decrease in the CdS thickness from 1500Å to 600 Å reduces both absorption and reflectance, resulting in a steep reduction in photocurrent loss. However, further decrease in the CdS thickness below 600 Å introduces an additional photocurrent loss due to increased reflectance, which slows down the rate of decrease in photocurrent loss. Besides, reducing the CdS thickness below 600 Å in a real cell may be risky because of the possibility of pin-holes in very thin CdS films which can cause low shunt resistance and degrade V_{oc} and fill factor.[11,12]

In order to study the effect of CdS thickness on the CdTe cell performance, CdTe solar cells with 650 Å and 1600 Å thick CdS layers were fabricated and tested (Table 6.1).

It was found that when the CdS thickness was lowered from 1600 Å to 650 Å, the J_{sc} increased by about 1.4 mA/cm^2 due to the combination of reduced reflectance (Figure 6.2) and absorption in CdS. Notice that the measured increase in J_{sc} (1.4 mA/cm^2) is lower than the predicted value of 3 mA/cm^2 in Figure 6.1 c. This is because, in our cells,

TABLE 6.1: Cells parameters for different CdS thicknesses

CdS thickness	V_{oc} (volts)	J_{sc} (mA/cm$_2$)	R_s (Ω cm^2)	R_{sh} (Ω cm^2)	FF	Eff (%)
650 Å	0.71	25.01	6.12	556	0.55	9.80
1600 Å	0.74	23.58	4.17	1108	0.61	10.62

when we try to thin the CdS layer below 1000 Å, some of the photo-generated carriers are lost due to low shunt resistance or pin-hole induced recombination. The lower values of shunt resistance, fill factor, and V_{oc} of the CdTe cell in Table 6.1 with 650 Å CdS supports the above conclusion. The reduction of CdS thickness below 600 Å is expected to cause even more pin-holes and non-uniformity problems, and may not result in a significant current gain because of the increased reflectance. Therefore, even though from theoretical viewpoint, the CdS thickness should be as small as possible, the practical optimum CdS thickness seems to be about 600-700 Å for achieving high J_{sc} and efficiency in the CdTe solar cells. The above guidelines match the structure of the highest efficiency (15.8 %) CdTe solar cell today which consists of 700 Å thick CdS layer.[12] It should be recognized that the practical optimum CdS thickness could be a function of CdS film quality, because higher pin-hole density will require thicker CdS films.

6.5.3 Effect of SnO_2 Thickness on Photocurrent Losses

Two additional sets of simulations were performed by fixing the CdS thicknesses

at 600 and 1200 Å and varying the SnO_2 thickness in the range of 700 Å to 12000 Å. Again, attempts were made to obtain reflectance minima at λ=6000 Å, which is close to the peak in the solar spectrum. Notice that the 600 Å thick CdS is close to the optimum CdS thickness (575.6 Å) determined from equation (6), which provide a local minimum in the reflectance at the desired wavelength. The 1200 Å thick CdS satisfies $n_2d_2 = 1/2 \lambda$ criteria in conjunction with quarter wavelength thick SnO_2 ($n_1d_1 = 1/4 \lambda$) to form a double minima (W-shaped) in the reflectance curve. The corresponding reflectance-induced photocurrent loss for the two cases, which calculated from the simulated reflectance spectrum, are shown in Figure 6.3. The data clearly indicates that there is about 0.8-0.9 mA/cm^2 difference in the minimum and maximum values of photocurrent loss. Figure 6.3 also indicates that the photocurrent loss is lower for the V-shaped reflectance profiles (CdS = 600 Å curve) compared to the W-shaped profiles (CdS = 1200 Å curve). This is because the W-shaped profile has a local maximum at 6000 Å and the two minimum points are located outside the CdTe cell absorption window (4000-9000 Å). Notice that when the SnO_2 thickness increases beyond 4000 Å, which is generally needed and used in current CdTe solar cells in order to reduce resistive losses, photocurrent loss due to reflectance does not change much with the SnO_2 thickness.

Some absorption measurements were also performed on the SnO_2 films to determine the photocurrent loss due to absorption in SnO_2. It was found that, on the average, about 15% of incident light is absorbed in a 10000 Å thick layer. Thus, reducing SnO_2 thickness could indeed reduce the photocurrent loss due to absorption, however, the increase in resistive loss due to thinner SnO_2 film could lower the J_{sc} and cell performance. Therefore, because of the competition between absorption and resistive losses, and the insensitivity of reflectance induced photocurrent loss when SnO_2 thickness is increased beyond 4000 Å, we conclude that the CdS film thickness is more critical than the SnO_2 thickness for achieving higher J_{sc} in the CdTe solar cells.

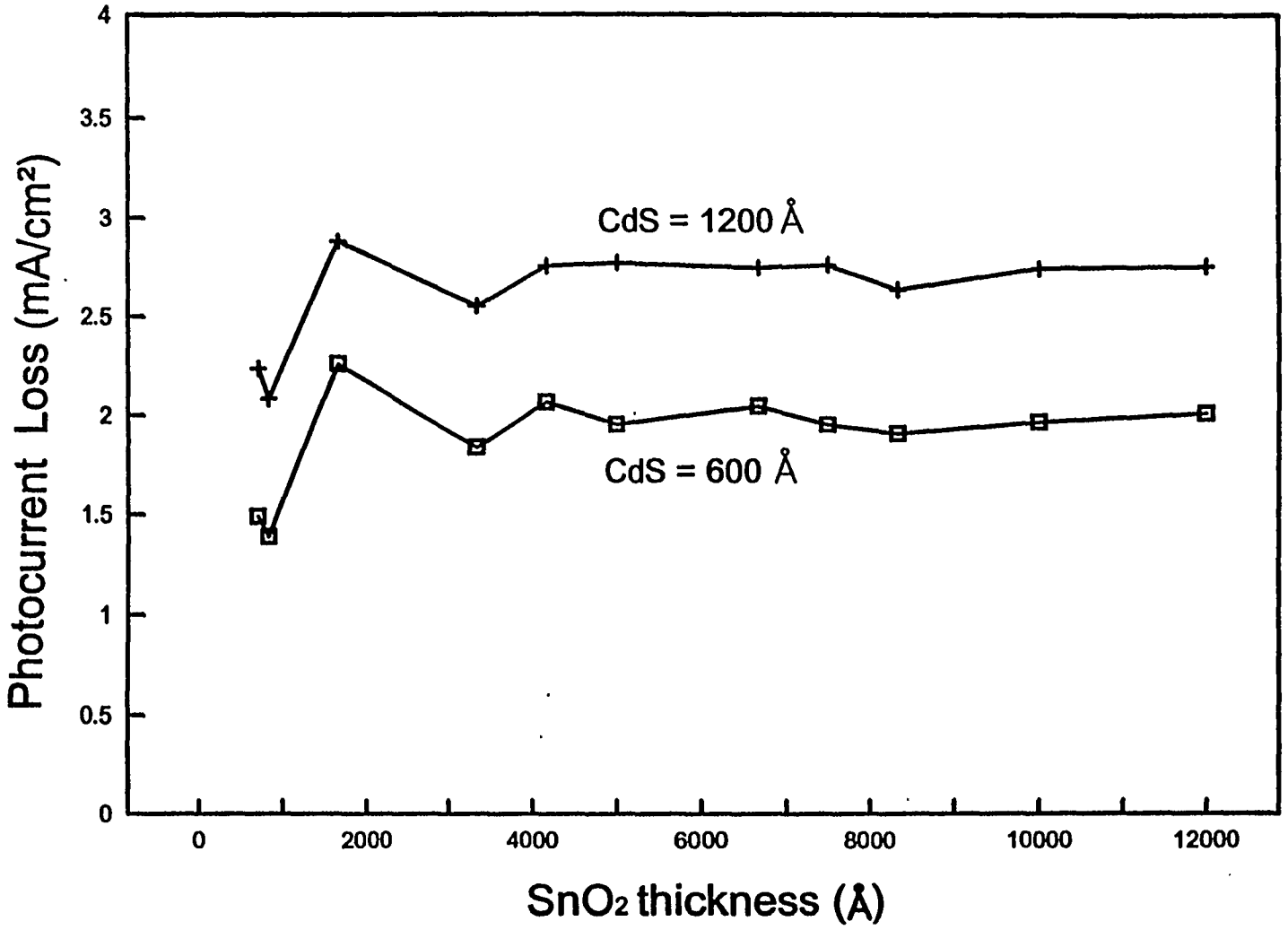

FIGURE 6.3: Photocurrent loss in CdTe solar cells due to the reflection with varying SnO_2 thicknesses

6.5.4 Minimization of the Front Glass Surface Reflectance

Even if the thicknesses of the CdS and SnO_2 layers were optimized to reduce the reflectance, there is still about four percent of incident light that is reflected from the air/glass interface (n=1.5 for glass). This reflectance corresponds to about 1.2 mA/cm^2 current loss in the CdTe solar cells under AM 1.5 illumination. Therefore, an appropriate AR coating layer on the glass substrate should improve the CdTe cell performance. Model calculations showed that in order to obtain zero reflectance, using equation 2 with $n_0=1$ for air, $n_2=1.5$ for glass, the optimum refractive index n_1 and thickness d_1 should be approximately 1.225 and 1224 Å, respectively. The corresponding reflectance is calculated and shown in Figure 6.4 a, as a function of wavelength. It was found that such a coating could reduce the photocurrent loss from 1.2 mA/cm^2 to 0.13 mA/cm^2. Since the material with $n_1=1.225$ is not readily available for the AR coating application, Magnesium Fluoride, with n_1 = 1.38, was deposited on the glass surface. MgF_2 is widely used as an AR coating material for Si solar cells. A combination of modelling and experimental data was utilized to understand how and to what extent the MgF_2 AR coating can improve the short circuit current of the CdTe cells. The simulated reflectance of a single layer MgF_2 coating on glass is also shown in Figure 6.4 b. The reflectance curves in Figure 6.4 were calculated to obtain minimum reflectance at $\lambda=6000$ Å, using the guideline $n_1d_1 = \lambda/4$. This reflectance data was then utilized to calculate (equation 1) the corresponding photocurrent loss (Table 6.2 a). The calculations predict that the J_{sc} of a CdS/CdTe cell should increase by about 0.7 mA/cm^2 as a result of 1087 Å MgF_2 AR coating. In order to verify the above results experimentally, about 1100 Å MgF_2 was evaporated on the glass side of the CdTe solar cells and the reflectance as well as short circuit current density were measured before and after the AR coating (Figure 6.5). These measured spectra were also used to calculate the corresponding photocurrent loss, listed in Table 6.2 (b). Notice that the shapes of measured and calculated reflectance curves (Figure 6.4 & 6.5) are slightly different because the simulation ignores any interference from SnO_2/CdS/CdTe films below the thick glass plate. This difference is also reflected

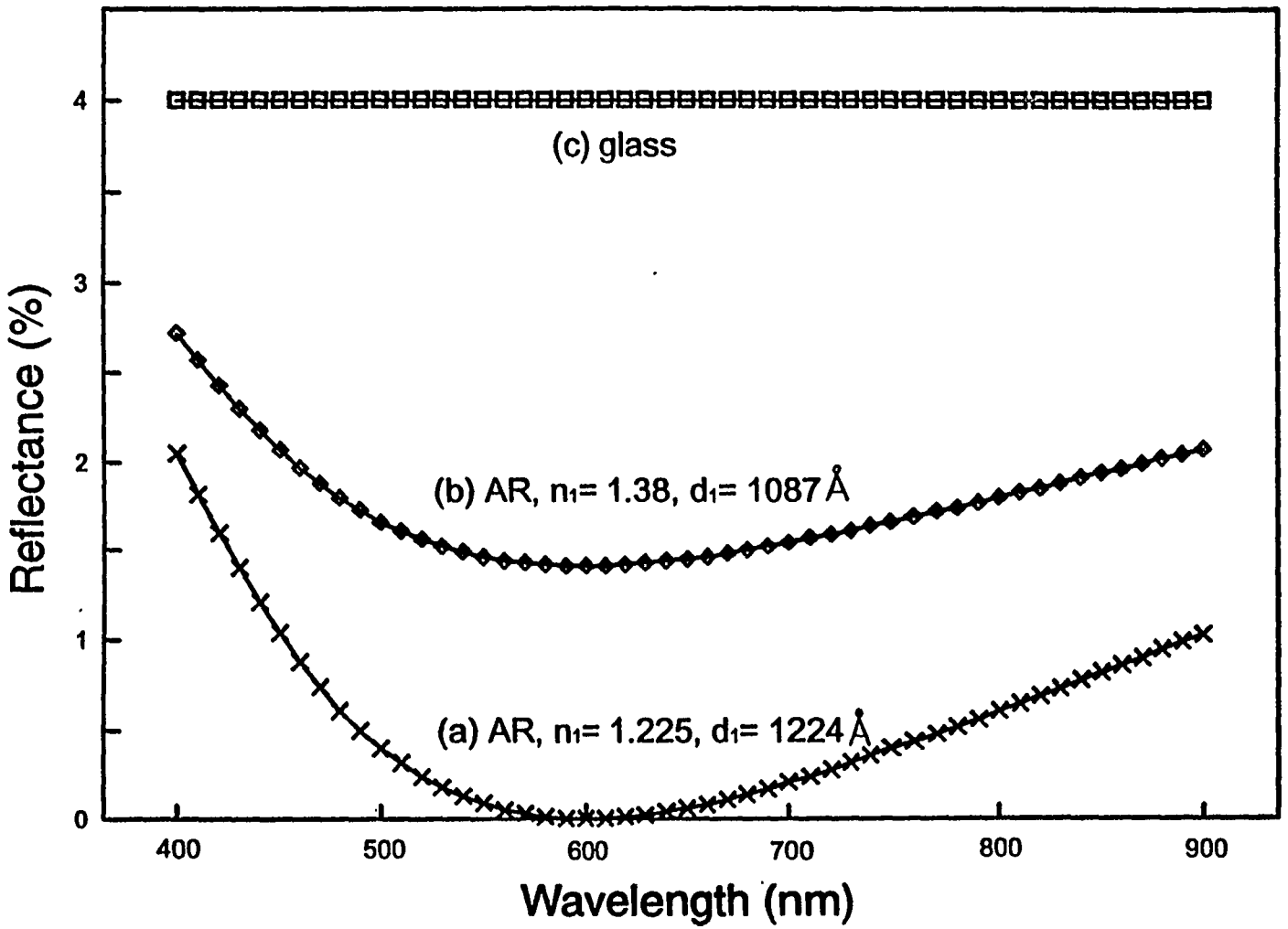

FIGURE 6.4: Calculated reflectance with two different AR coatings on glass

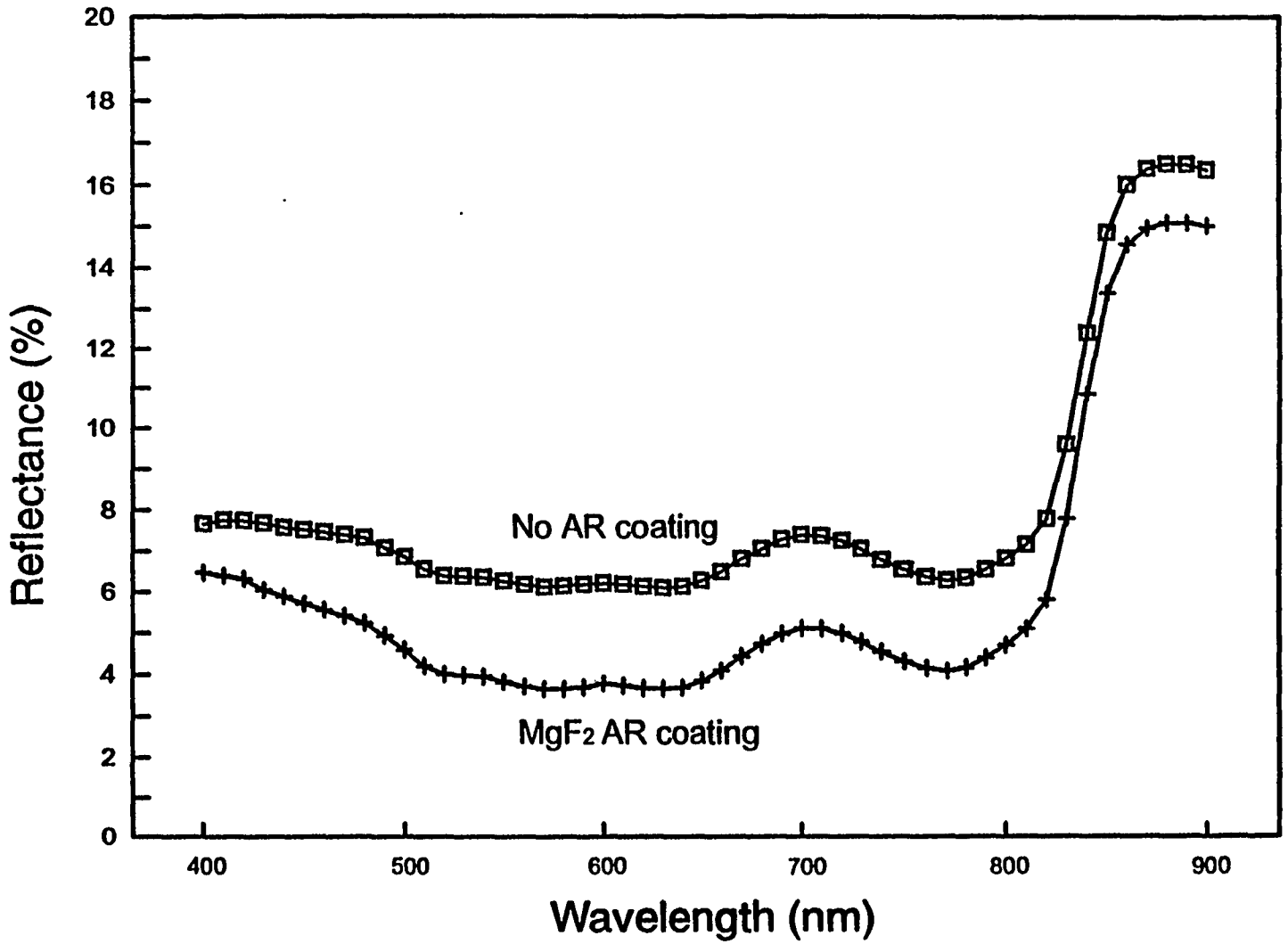

FIGURE 6.5: Measured reflectance for CdTe/CdS solar cells with and without AR coating

in the photocurrent losses of Table 6.2. However, since such effect should be the same before and after the AR coating, the simulated current gain of 0.7 mA/cm^2 agrees well with the gain calculated from the measured reflectance (Table 6.2). This also agrees well with the increase in J_{sc} from 23.1 mA/cm^2 (before AR coating) to 23.6 mA/cm^2 (after AR coating). The slight difference between measured and calculated increase in J_{sc} could result from the assumed 100% internal quantum efficiency (IQE) in the simulation.

TABLE 6.2: Photocurrent losses before and after AR coating from

(a) simulated reflectivity spectrum

(b) measured reflectivity of a practical cell

Conditions	Photocurrent Losses (mA/cm^2)	Current gain from AR coating
(a) Current loss calculated from the simulated reflectivity spectrum		
Glass only	1.24	-
t_{MgF2} = 1087 Å (min reflectance at 6000 Å)	0.52	0.72
(b) Current loss calculated from the measured reflectivity of a practical cell		
Before MgF_2 coating	2.41	-
After MgF_2 coating	1.75	0.67

6.6. Conclusion

Attempts were made to simulate and measure the photocurrent loss in the CdTe solar cells due to the CdS and SnO_2 thickness, before and after an antireflection coating. The effects of CdS thickness on the reflectance and photocurrent loss were investigated and it was found from the simulation that the reduced reflectance could increase J_{sc} by about 1 mA/cm^2, if the CdS thickness is reduced to 600 Å. These results were verified

by fabricating CdTe solar cells with CdS thicknesses of 1600 and 650 Å. It was found that the optimum CdS thickness is about 600-700 Å for achieving high J_{sc} in a practical CdTe solar cell, because at this thickness, it benefits from both reduced absorption and reflectance without the risk of pin-holes formation. Reducing the CdS thickness below 600 Å increases the reflectance losses and may not give a significant increase in J_{sc} due to reduced absorption because pin-holes formation tend to degrade the cell performance. It was found that the control of CdS film thickness is more critical than that of the SnO_2 because the reflectance does not change much when the SnO_2 thickness exceeds 4000 Å, which is used by most investigators today to minimize the series resistance. Finally, optimum MgF_2 thickness on glass was found to be 1100 Å which should give about 0.7 mA/cm^2 additional increase in J_{sc}. This value agrees with the measured results from CdTe solar cells.

Acknowledgement

The authors would like to thank to Dr. R. R. Arya and L. Russell of Solarex Corp. for the growth of CdS and SnO_2 films. This work was supported by National Renewable Energy Laboratory under contract No. XG-2-11036-3.

References

1. R. H. Bube and K. W. Mitchell, J. Electron. Mater. **22**, 17 (1993).
2. P.V. Meyers, Solar Cells **27**, 91 (1989).
3. A. Rohatgi, S.A. Ringel, R. Sudharsanan, and H.C. Chou, *Proceedings of the 22nd IEEE Photovoltaic Specialists Conference* (1991), p. 962.
4. T.L. Chu, S.S. Chu, C. Wang, C. Ferekides, J. Britt, C.Q. Wu, and H.S. Ullal, IEEE Electron Device Lett. **13**, 303 (1992).
5. A. K. Bhat, Ph.D. Thesis, University of Toledo, (1991), p. 61.
6. M. A. Green, *Solar Cells* (Prentice-Hall, Englewood Cliffs, 1982).
7. A. Thelen, Optic **13**, 537 (1956).

8. O. S. Heavens, *Optical Properties of Thin Solid Films* (Butterworths, London, 1955).

9. B. H. Billings, Ed., *American Institute of Physics Handbook*, 2nd ed. (Mcgraw-Hill, New York, 1963), p. 9-50.

10. SD Series Ellipsometers User Manual, Thin Film Measurement Systems (PLASMOS GmbH, Munich, Germany, 1990).

11. T. Arita, A. Hanafusa, N. Ueno, Y. Nishiyama, and S. Kitamura, Solar Energy Materials **23**, 371 (1991).

12. C. Ferekides, J. Britt, Y. Ma, and L. Killian, *Proceedings of the 23rd IEEE Photovoltaic Specialists Conference* (1993), p. 389.

7. Investigation of the effects of various film processing parameters on cell performance

7.1 Effect of temperature during H_2 treatment of CdS films

Oxygen in CdS grain boundaries is known to be a detrimental recombination center. Heat treatment of the CdS films in H_2 ambient in the MOCVD reactor, prior to CdTe deposition, is routinely done in order to remove oxygen and oxygen related defects. It was reported earlier[1] that the treatment also leaves Cd-deficient region on the CdS surface, and it was therefore felt that the temperature used for the heat treatment should be optimized to ensure that the CdS films are stoichiometric. Starting with different solution grown CdS films, a series of experiments were performed to investigate the effect of the temperature on cell performance.

One set of the CdS films chosen was grown using a thiourea concentration of 0.01 M (thiourea rich) and a $CdCl_2$ concentration of 0.002 M. Another set of CdS films were grown at a slower rate using both thiourea and $CdCl_2$ concentrations of 0.002 M. It was observed that the optimum temperature during H_2 treatment depends on the concentrations of the reactants used. Specifically, both V_{oc} and fill factor were highest (Figure 7.1) when the annealing was done at 425°C for films that were grown using a thiourea concentration of 0.01M. However, for CdS films grown using a thiourea concentration of 0.002 M (slow growth and possibly Cd-rich films), the fill factor and efficiencies improved as the temperature was increased to 475°C. This result is consistent with our earlier conclusion that the heat treatment in H_2 ambient drives out some Cd along with O from the surface.

7.2 Spin-coating of $CdCl_2$ solution on CdTe film

In order to ensure better uniformity of $CdCl_2$ treatment on CdS/CdTe films, several samples were selected for application of $CdCl_2$-methanol solution (0.5 g $CdCl_2$ in 100 ml methanol). Sample #1 underwent the regular method of $CdCl_2$ treatment in which 7

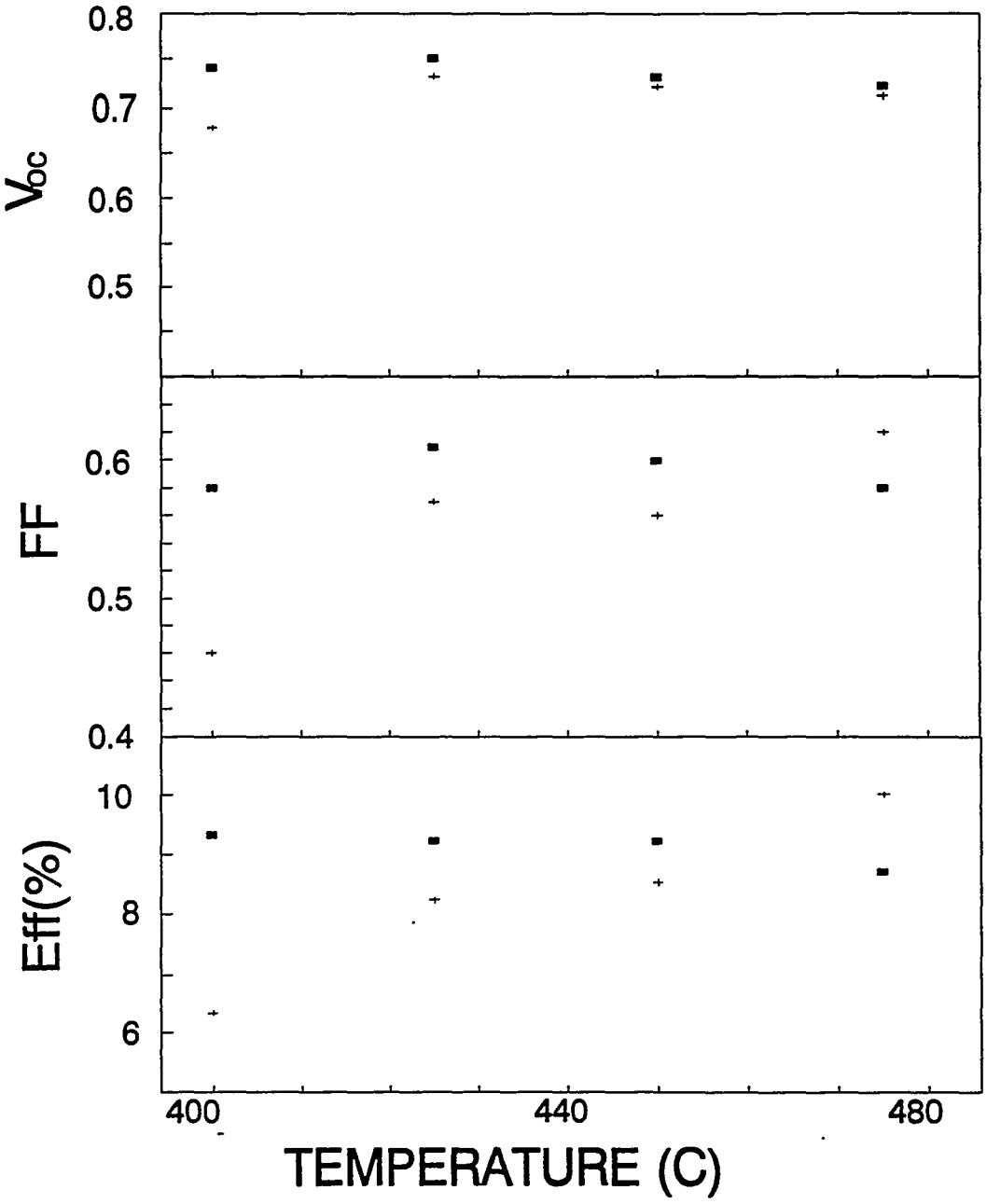

FIGURE 7.1: Effect of temperature during H_2 treatment of CdS films on (a) V_{oc}, (b) fill factor, and (c) cell efficiency; 0.01 M thiourea (▬), 0.002 M thiourea (+) in bath solution

drops of $CdCl_2$ solution were added to the sample which was placed on a hot plate. The sample was then annealed at 400°C for 30 minutes in N_2-O_2 mixture. The remaining samples were treated with 7 drops of $CdCl_2$ on a variable-speed spinning wheel. The $CdCl_2$ treatment was followed by annealing in a furnace, under conditions similar to that for sample #1. Cell fabrication was then completed, as usual, by evaporating Cu/Au contacts. The results of this experiment are given in Table 7.1.

TABLE 7.1: Effect of spin-coating of $CdCl_2$ on cell performance

I.D #E0524	1	9	0	2	11
Condition for $CdCl_2$ treatment at 0.5 $CdCl_2$	Normal	500 rpm	2000 rpm	3000 rpm	4000 rpm
V_{oc} (volts)	0.72	0.72	0.71	0.75	0.71
J_{sc} (mA/cm^2)	20.9	22.1	21.0	20.9	20.5
FF	0.62	0.6	0.61	0.64	0.61
Eff (%)	9.4	9.5	9.0	10.0	9.0

More experiments were performed with different concentrations of $CdCl_2$ solutions and a range of spinning speeds. However, no clear trend was observed. In most instances, even when the application of $CdCl_2$ is visibly non-uniform, the performance of the cells is not affected.

7.3 Additional experiments and collaborative efforts

A number of experiments were carried out to re-evaluate the processing methods that are currently in use. For example, different annealing durations and ambients were

tried for annealing CdS, CdS/CdTe, and CdS/CdTe/Cu/Au films. In some instances, sample cooling after the annealing step was carried out in the furnace to reduce possible deleterious effects of humidity and impurities in the air. The thickness of CdTe was also varied from the usual value of about 2.6 μm (Table 7.2). However, no improvement in cell efficiency resulted from any of these variations.

The optimized processing steps in use for our CdS/CdTe cells are as follows:

a) 450°C anneal in N_2 of solution grown CdS films for 50 minutes,

b) 450°C anneal in H_2 of CdS films in MOCVD reactor for 18 minutes prior to CdTe growth,

c) 400°C anneal in 20% O_2 in N_2 of CdS/CdTe films for 30 minutes,

d) 150°C anneal in Ar of CdS/CdTe/Cu/Au films for 60 minutes.

TABLE 7.2: Effect of CdTe film thickness on cell performance

Run ID# (E110693)/Cell#	2	5	8
CdTe Thickness/Deposition Time	2.6 μm/60 min.	3.5 μm/95 min.	4.8 μm/130 min.
V_{oc} (volts)	0.73	0.72	0.73
J_{sc} (mA/cm^2)	21.6	20.9	21.1
R_s (Ω cm^2)	3.9	4.5	4.7
R_{sh} (Ω cm^2)	461	348	522
FF	0.56	0.52	0.49
Eff (%)	8.8	7.9	7.5

In another set of experiments, the 2.6 μm MOCVD CdTe film growth was completed in two stages - each stage consisting of a heat treatment in H_2 for 18 minutes at 450°C and CdTe growth for 35 minutes at 400°C. Preliminary results, shown in Table 7.3, suggest that the two-step process has positive effect on cell performance. This variable is being investigated further.

Table 7.3: Comparison of single-step and two-step CdTe growth

Run ID# F013194	#5 One Step deposition (growth time = 70 min)		#6 Two Step deposition (growth time = 35 + 35 min)	
DOT	1	2	1	2
V_{oc} (volts)	0.70	0.70	0.72	0.71
J_{sc} (mA/cm$_2$)	20.6	20.7	21.0	21.1
R_s (Ω cm^2)	3.9	4.0	3.4	3.9
R_{sh} (Ω cm^2)	774	536	1080	1151
FF	0.60	0.58	0.63	0.63
Eff (%)	8.7	8.4	9.5	9.5

Effect of different SnO_2 substrates on cell performance

In selected instances a comparison was made between Solarex (with textured, medium textured and untextured SnO_2-coatings), Ashai (untextured), Nippon (untextured) and LOF (medium textured 8,10 & 20 $\Omega/\square$) SnO_2 substrates. Table 7.4 shows the cell efficiencies achieved on these different glass/SnO2 substrates.

The results reveal that the textured Solarex glass/SnO_2 substrate is the most suitable substrate for our fabrication process. However, the CdS film thickness required is higher when highly textured substrates are used (Tables 7.5 & 7.6).

TABLE 7.4: Effect of different SnO_2 substrates on cell performance

Source	Solarex			Ashai	Nippon	LOF		
Type	Text	Medium Tex	Untext	Untext	Untext	Flat 8 Ω/□	Flat 10 Ω/□	Flat 20 Ω/□
ID#	A-27	A-34	A-61	A-73	A-2	A-68	B-15	B-14
V_{oc}	0.75	0.69	0.74	0.66	0.69	0.73	0.75	0.76
J_{sc}	24.6	23.2	24.1	21.0	20.5	21.0	19.92	22.4
R_s	3.3	15.1	4.0	13.0	4.8	3.3	4.34	6.14
R_{sh}	1434	409	1138	141	737	589	696	2623
FF	0.66	0.55	0.61	0.45	0.57	0.61	0.62	0.61
Eff	11.9	8.9	10.9	6.3	8.0	9.4	9.38	10.3

TABLE 7.5: Effect of CdS film thickness for Solarex untextured SnO_2/glass substrates

CdS thickness	650 Å	1600 Å
V_{oc} (volts)	0.71	0.74
J_{sc} (mA/cm^2)	25.0	23.6
R_s (Ω cm^2)	6.2	4.2
R_{sh} (Ω cm^2)	556	1108
FF	0.55	0.61
Eff (%)	9.8	10.6

TABLE 7.6: Effect of CdS film thickness for Solarex textured SnO_2/glass substrates

CdS thickness	850 Å	2000 Å
V_{oc} (volts)	0.60	0.72
J_{sc} (mA/cm^2)	24.0	23.0
R_s (Ω cm^2)	4.5	3.2
R_{sh} (Ω cm^2)	202	760
FF	0.52	0.61
Eff (%)	7.5	10.2

Additionally, some experiments were carried out in collaboration with other groups that are working with polycrystalline CdTe films, including Solar Cells Inc., Spire Corporation, and The University of Toledo. Devices at various stages of completion were exchanged in order to see whether the efficiency limiting steps could be identified. However, such efforts were not conclusive and did not result in higher efficiency, possibly because the optimum conditions which must be used to complete the remaining processing steps depend on the processes used in the preceding steps.

In summary, extensive emperical investigation of process variables did not result in significant improvement in CdTe cell efficiency. This indicates that there is a need for fundamental understanding of loss mechanisms in CdTe/CdS cells. Experiments and detailed analysis of cells is underway to improve cell performance by a combination of emperical and fundamental investigation of CdTe solar cells.

References

1. A. Rohatgi, International Journal of Solar Energy, Vol. 12, p 37 (1992).

8. Solution Growth of CdTe

Solution growth of II-VI films such as CdS and CdSe has been reported by several authors[1]. The technique involves the formation of cadmium complexes, which gradually release Cd^{2+}, and the simultaneous release of the S^{2-} or Se^{2-} to form the II-VI compounds. A similar technique for making CdTe films would be possible, if a source of Te^{2-} is made available. However, compounds such as thiourea which can release S^{2-}, and sodium selenosulphate which can release Se^{2-}, are not available to provide Te^{2-}. Therefore, a technique which involves the in-situ production of H_2Te is being investigated.

This technique involves the electrolytic production of H_2Te using 50% sulfuric or phosphoric acid as the electrolyte, a platinum anode, and a tellurium cathode. Our goal is to use the H_2Te gas and an aqueous solution of $CdCl_2$ to form CdTe films (See Figure 8.1). However, certain difficulties faced in this process, which will be discussed here, must be solved if this technique is to be used successfully.

Electrolytic production of H_2Te

H_2Te has a boiling point of -2°C, is extremely unstable and rapidly decomposes into elemental tellurium in the presence of oxygen. Because of its instability, the gas is not available commercially and must be prepared in situ. Electrolytic production of H_2Te has been reported in the literature, probably for the first time, more than eighty years back[2].

The electrolysis can be described by the following equations:

$H_2O \leftrightarrows H^+ + OH^-$

$4OH^- \leftrightarrows 2H_2O + O_2 \uparrow + 4e^-$ (at platinum anode)

$2H^+ + Te + 2e^- \leftrightarrows H_2Te \uparrow$ (at tellurium cathode).

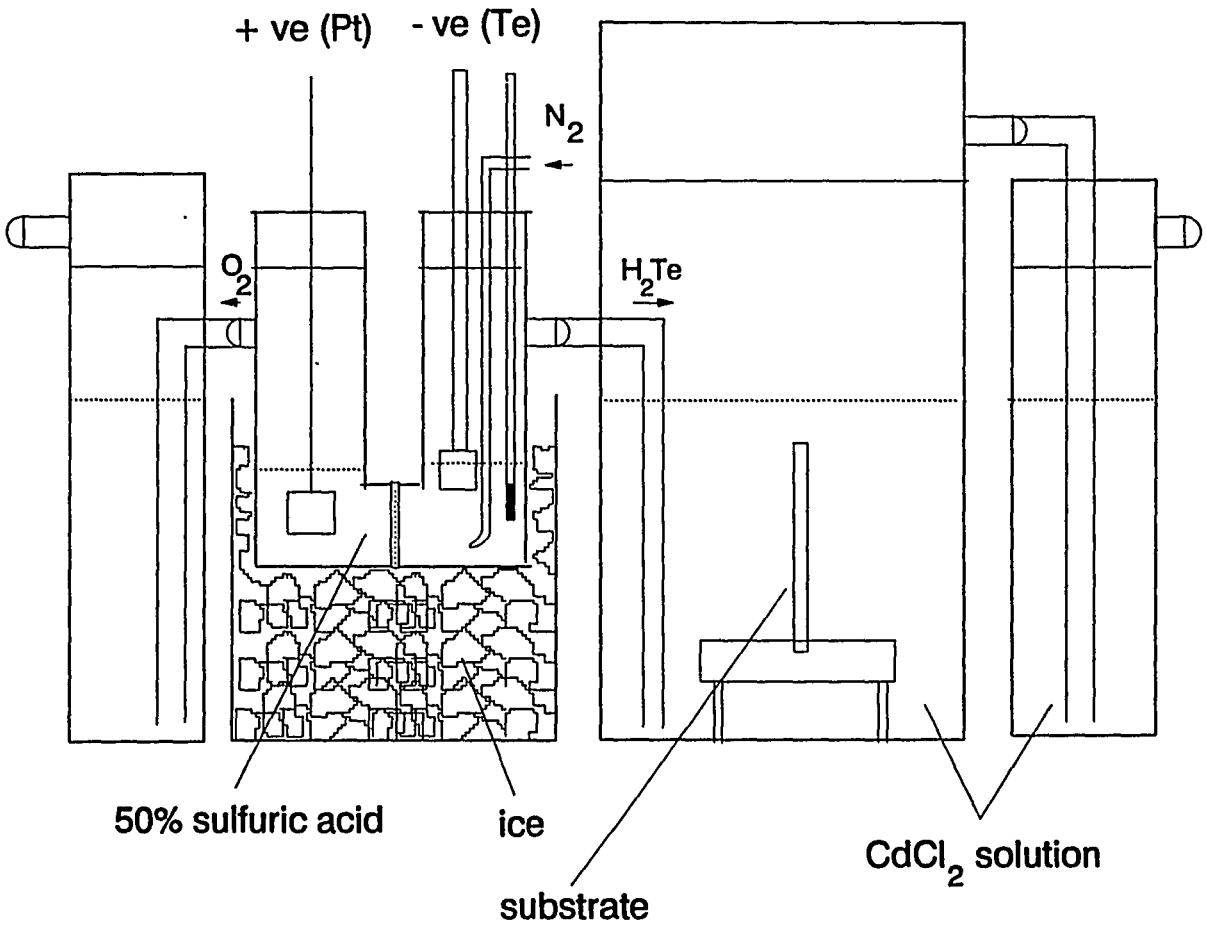

FIGURE 8.1: Equipment for solution growth of CdTe using electrolytic production of H_2Te

Solution growth

Heavy metal tellurides, such as cadmium telluride, can be prepared by the hydrogen telluride treatment of an aqueous solution of a suitable salt, such as chloride, sulphate, or nitrate. The reaction which occur is represented by the equation

$$CdCl_2 + H_2Te \leftrightarrows CdTe \downarrow + 2HCl.$$

The above reaction has been reported in the literature by several authors[3]. However, the reaction has been described only in the context of preparing precipitates of CdTe. Our goal in this project is to study the suitability of the solution growth technique for preparing thin film CdTe.

The technique looks attractive because it is simple and inexpensive. The reactions are carried out at atmospheric pressure, and moderate temperatures (electrolysis at 0°C, and solution growth at ambient temperatures). Good uniformity of films can be expected through vigorous stirring of the reaction mixture during film growth. The main problem, as noted above, is the rapid decomposition of H_2Te into Te.

Experiments

After some initial difficulties, the electrolytic cell used as a source of H_2Te gas worked satisfactorily. N_2 was used as a carrier gas, and also to purge the reaction vessel of O_2. However, the H_2Te when bubbled through the reaction vessel containing the $CdCl_2$ solution gave precipitates of Te and CdTe. No deposition was observed on the glass substrates placed in the reaction vessel. When ammonia was added to the reaction mixture in order to form an ammonium complex of Cd, thereby reducing the availability of Cd^{2+} ions, gradual precipitation of a reddish brown particulates was observed. It appears that the H_2Te decomposes spontaneously in the presence of dissolved oxygen to give elemental tellurium. The presence of Te particles in the solution further leads to homogenous precipitation of CdTe from the solution. We believe that the mechanism for the process is the following:

$$H_2Te \rightleftarrows H^+ + HTe^-$$

$HTe^- \rightleftarrows H^+ + Te^{2-}$

$4Te^{2-} + O_2 + 2H_2O \rightleftarrows 4Te + 4OH^-$

Different methods were attempted in order to suppress the precipitation of Te. The deionized water used to make the aqueous solution was boiled before use to remove some of the dissolved oxygen (typically 10 mg/liter). However, heating the water to boiling point helps remove less than half of the dissolved oxygen, and was found to be insufficient. Therefore, a small amount of anhydrous sodium sulfite was used (95 mg/liter). Na_2SO_3 is a strong reducing agent and in the presence of Co^{2+} is known to remove the dissolved oxygen via the following reaction[4]:

$2Na_2SO_3 + O_2 \rightleftarrows 2Na_2SO_4$

However, even this method was not found to work satisfactorily.

It was discovered that bubbling the H_2Te through a strong basic solution prevents precipitation. It appears that in the presence of a strong base (high OH^- concentration), the last reaction in the set of three reactions stated above is suppressed, thus preventing formation of Te precipitates.

NaOH and NH_4OH were used to make the desired basic solutions. Na_2Te, which is formed when NaOH is used, is more stable compared to the H_2Te solution because of the presence of OH^-. The following reactions can be reportedly[5] used to prepare CdTe precipitates, while inhibiting the formation of elemental Te:

$H_2Te + 2NaOH \rightleftarrows Na_2Te + 2H_2O$

$Na_2Te + CdCl_2 \rightleftarrows CdTe + 2NaCl$

It was found that the amount of NH_4OH or NaOH required to prevent precipitation is less when anhydrous Na_2SO_3 is used simultaneously to remove the dissolved oxygen. However, there are certain difficulties that remain to be tackled. NH_4OH when added to the $CdCl_2$ solution gives a cadmium ammonium complex which is soluble and does not readily release Cd^{2+}, which we believe is necessary to form thin films (as in the case of CdS or CdSe[1]). No precipitation or deposition is observed for several hours, after which a brownish precipitate appears. On the other hand, addition of NaOH gives rise to rapid

precipitation of $Cd(OH)_2$ due to its low solubility. The $Cd(OH)_2$ precipitates then provide nucleating centers for more precipitation of Te and CdTe. A few combinations of NH_4OH and NaOH have also been tried, without much success.

It is not clear at this point as to exactly what steps should be taken to overcome the existing problems. One possibility is to use hydrazine, which is an extremely powerful reducing agent, in the reaction mixture to prevent the oxidation of H_2Te. Although, hydrazine has been reportedly successfully used to grow CdTe films, starting with TeO_2 as source of tellurium[6], we have avoided use of hydrazine because it is highly toxic.

References

1. A. Mondal, T.K. Chaudhuri, and P. Pramanik, Solar Energy Materials, 7 (1983), 431-438.
2. L.M. Dennis and R.P. Anderson, J. Am. Chem. Soc. 36, 882 (1914).
3. C.A. Tibbals, J. Am. Chem. Soc., 31, 902 (1909).
4. American Public Health Association, 14_{th} edition, " Standard Methods for the Examination of Water and Wastewater" 1975, p85.
5. I.K. Taimni and Ram Rakshpal, Chimie Analytique, Vol. 46, No 4 (1964).
6. G.K. Padam and G.L. Malhotra, Mat. Res. Bull., Vol. 24, pp. 595-601 (1989).

9. Thin-Film Single Crystal CdTe Solar Cells

In order to understand the loss mechanisms and some of the intricacies of polycrystalline CdTe/CdS cells, attempts are being made to fabricate CdTe/CdS cells comprising single crystal CdTe films by the lift-off process. CdTe films will be grown on GaAs substrate to evaluate the quality of the single crystal CdTe films. The CdS and SnO_2 films will be deposited on top of CdTe film by solution growth and sputtering, respectively. In order to fabricate the solar cells, the GaAs substrate has to be separated from the CdTe film. Therefore, an etchant that selectively etches GaAs rapidly but does not attack CdTe film has to be found.

Several etchants for GaAs are based on the use of H_2O_2 in combination with an acid or base to oxidize and dissolve GaAs. H_2SO_4, H_3PO_4, HNO_3, HCl, and citric acids as well as NH_4OH and NaOH, have all been used for this purpose. Unfortunately, some of these etches also etch the CdTe film. Therefore, it was necessary to look for a more selective etch. Since common etchants such as HNO_3, HCl, HF with H_2O_2, and Br_2-MeOH solutions attack CdTe, these were not suitable for our purpose. We investigated H_2SO_4, H_3PO_4, citric acids and NaOH to develop a selective etch for etching GaAs without attacking CdTe. The preliminary results are shown below:

(1) H_3PO_4 (85 wt. %) : H_2O_2 (30 wt. %) : H_2O

(a) $H_3PO_4 : H_2O_2 : H_2O = 30:50:20$

CdTe: rapid etching of 2 μm films (< 1 min)

GaAs: no observable change

(b) $H_3PO_4 : H_2O_2 : H_2O = 25:15:60$

Reduced amount of H_2O_2 slows down reaction with CdTe

CdTe: still fast etching of 2 μm films (about 1.5 min)

GaAs: no observable change

(2) Citric acid (50 wt. %) : H_2O_2 = 10:1

CdTe: fast etching of 2 μm films (about 2 min), but no observable change for the CdS film underneath

GaAs: no observable change

(3) $H_2SO_4 : H_2O = 5:1$

After 4 hours:

No observable changes for CdTe and GaAs

After 48 hours:

CdTe : film peeled off, seems the etchant reacts with CdS but not CdTe

GaAs : Thickness of wafer changed from 34.4 mil to 33.6 mil, etch rate = 0.017 mil/hour

(4) NaOH (5 wt. %) : H_2O_2 = 5:1

After 3 hours :

CdTe : No observable change

GaAs : Thickness of wafer changes from 33.8 mil to 20 mil, etch rate = 4.6 mil/hour (11.68 μm/hour)

After 24 hours :

CdTe : No observable change

GaAs : Wafer dissolved

Based on the above results, NaOH-H_2O_2 etchant was found to be the best candidate for selective etching. Another observation, which could prove useful in the future, was that a mixture of citric acid and H_2O_2 could selectively etch CdTe without dissolving CdS. Samples of SnO_2/CdS/CdTe/GaAs structures with different CdTe growth conditions will been prepared. After putting the black wax on the top, these samples will be subjected to NaOH : H_2O_2 etch, followed by film transfer. Finally, single crystal thin film CdTe solar cell will be completed by contact deposition (Figure 9.1).

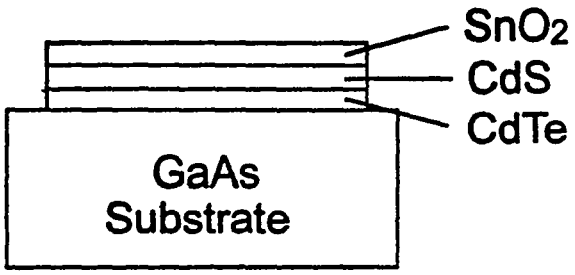

(a) Grow CdTe, CdS and SnO2 on GaAs substrate

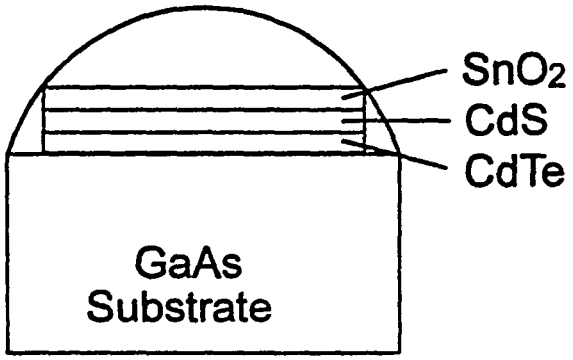

(b) Put black wax on the top

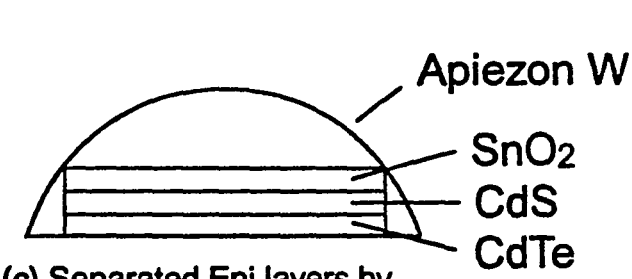

(c) Separated Epi layers by selective etch GaAs

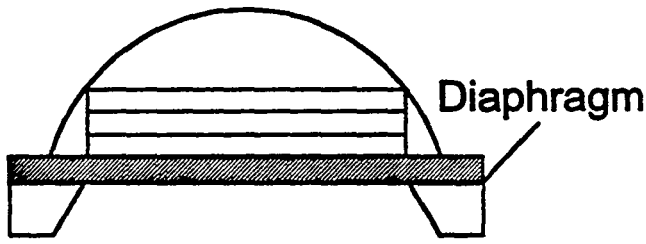

(d) CdTe/CdS/SnO2 films bring on diaphragm

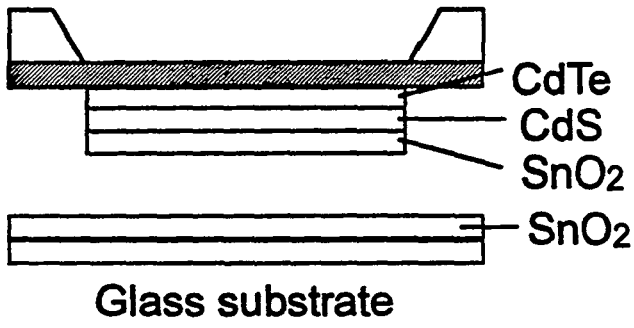

(e) Transfer layers to substrate

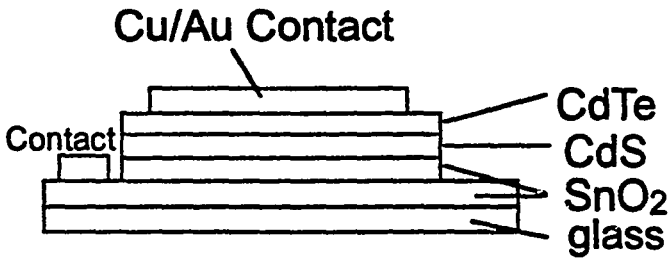

(f) Complete subsequent cell fabrication

FIGURE 9.1: Steps in the fabrication of thin film single crystal CdTe cells

10. Summary

An attempt has been made to improve the fundamental understanding of the efficiency limiting defects and mechanisms in order to reduce the gap between current and practically achievable efficiency of polycrytalline thin film CdS/CdTe solar cells. In this study, CdTe/CdS solar cells were fabricated by depositing CdTe films on glass/SnO_2/CdS substrates by MOCVD in different growth ambients with Te/Cd mole ratios in the range of 0.02 to 6. The CdS films were made in an aqueous solution while varying the starting amounts of cadmium chloride and thiourea in the bath. The films and devices were analyzed using SIMS, I-V, C-V, and EBIC measurements. The best cell efficiencies in the range of 11.5% to 12.0% were obtained with a Te/Cd ratio of about six.

Detailed measurements and analysis revealed a high degree of atomic inter-diffusion at the interface when the CdTe films were grown in a Te-rich atmosphere. The current transport in the cells grown in Cd-rich ambient was found to be controlled by the tunneling/interface recombination mechanism, and the transport analysis showed that the depletion region recombination became dominant in the "Te-rich" cells. This suggests that the enhanced inter-diffusion reduces interface states which switches the transport mechanism. Other process parameters such as the temperature during H_2 annealing, and the contact metal evaporation rates and film thicknesses were studied, and were also found to be critical.

Rapid thermal processing was investigated as an alternative to the conventional post-growth furnace anneal of the CdS/CdTe films. An efficiency of 10.7% was recorded without use of $CdCl_2$ as a fluxing agent for CdTe grain regrowth. Simulations and direct measurements were made to determine the loss in photocurrent due to absorption in the CdS window layer and multiple beam interference. A solution growth process for making CdTe films was attempted. However, the problem of homogenous precipitation of Te and CdTe from the solution has not been solved yet.

Certain other process variables such as SnO_2 substrates, and CdS/CdTe

processing conditions were investigated emperically, but no clear trend was found toward efficiency improvement. Finally, in order to understand the loss mechanisms and some of the intricacies of the polycrystalline material, attempts are currently under way to fabricate CdTe/CdS cells comprising single-crystal CdTe films by the lift-off process.

REPORT DOCUMENTATION PAGE

Form Approved
OMB NO. 0704-0188

1. AGENCY USE ONLY (Leave blank)	2. REPORT DATE	3. REPORT TYPE AND DATES COVERED
	September 1994	Annual Subcontract Report, 1 January 1993 - 31 December 1993

4. TITLE AND SUBTITLE

Development of High-Efficiency, Thin-Film CdTe Solar Cells

5. FUNDING NUMBERS

C: XG-2-11036-3

TA: PV431101

6. AUTHOR(S)

A. Rohatgi, H. C. Chou, S. Kamra, A. Bhat

7. PERFORMING ORGANIZATION NAME(S) AND ADDRESS(ES)

Georgia Institute of Technology
School of Electrical and Computer Engineering
Atlanta, Georgia 30332-0250

8. PERFORMING ORGANIZATION REPORT NUMBER

9. SPONSORING/MONITORING AGENCY NAME(S) AND ADDRESS(ES)

National Renewable Energy Laboratory
1617 Cole Blvd.
Golden, CO 80401-3393

10. SPONSORING/MONITORING AGENCY REPORT NUMBER

TP-451-7065

DE94011885

11. SUPPLEMENTARY NOTES

NREL Technical Monitor: B. von Roedern

12a. DISTRIBUTION/AVAILABILITY STATEMENT

12b. DISTRIBUTION CODE

UC-1263

13. ABSTRACT *(Maximum 200 words)*

This report describes work to improve the understanding of the loss mechanisms in thin-film CdS/CdTe solar cells, and to improve their efficiency by characterizing the properties of the films as well as the finished devices. To accomplish this, solar cells were fabricated on glass/SnO_2 substrates by sequentially growing CdS films from aqueous solution, CdTe films by metal organic chemical vapor deposition (MOCVD), and Cu/Au films by evaporation. Several process parameters were varied to observe their effects on cell performance. The films and devices were characterized using secondary ion mass spectroscopy and measurements of I-V, C-V, I-V-T, and electron-beam-induced current. Rapid thermal processing was investigated as an alternative to the conventional $CdCl_2$ treatment and post-growth furnace anneal of the CdS/CdTe films. We also attempted to make CdTe/CdS cells comprised of single-crystal CdTe films made by the "liftoff" process. Finally, consistent with the long-term requirement of cost-effective, large-scale terrestrial applications of photovoltaics, we investigated a solution growth technique for depositing CdTe films.

14. SUBJECT TERMS

high efficiency ; thin films ; cadmium telluride ; photovoltaics ; solar cells

15. NUMBER OF PAGES

88

16. PRICE CODE

17. SECURITY CLASSIFICATION OF REPORT	18. SECURITY CLASSIFICATION OF THIS PAGE	19. SECURITY CLASSIFICATION OF ABSTRACT	20. LIMITATION OF ABSTRACT
Unclassified	Unclassified	Unclassified	UL